ELSEVIER

Journal of Hazardous Materials 44 (1995) 141–183

JOURNAL OF HAZARDOUS MATERIALS

A two-phase release model for quantifying risk reduction for modified HF alkylation catalysts

R. Muralidhar[a,*], G.R. Jersey[a], F.J. Krambeck[a], S. Sundaresan[b]

[a] *Mobil Research and Development Corporation, Paulsboro, NJ 08066, USA*
[b] *Chemical Engineering Department, Princeton University, Princeton, NJ 08544, USA*

Received 21 September 1994; accepted 7 April 1995

Abstract

This paper describes a two-phase jet model for predicting the HF rainout (capture) in HF/additive releases. The parent droplets of the release mixture constitute the first phase. The second phase is a vapor–liquid fog. The drops are not in equilibrium with the fog phase with which they exchange mass and energy. The fog at any location is assumed to be in local equilibrium. The fog-phase calculations account for HF oligomerization and HF–water complex equilibria in the vapor phase and vapor–liquid equilibrium in the fog. The model incorporates jet trajectory calculations and hence can predict liquid 'rainout' and the capture distance. The model HF capture predictions are in agreement with small and large scale HF/additive release experiments. The fog properties and flow rate may be used to initialize atmospheric fog dispersion models for use in risk assessment calculations.

Keywords: Aerosol; Multicomponent model; HF; Jet; Rainout

1. Introduction

Hydrogen fluoride (HF) is widely used in petroleum refining as a catalyst in the alkylation process [1]. Recently, there has been public concern about the safety of HF-based processes. This derives from tests [2] which have shown that a release of anhydrous HF (AHF) under typical alkylation conditions, results in almost all of the material becoming airborne as a toxic two-phase vapor–liquid fog. This complete aerosolization of HF is attributed to flash atomization, a process that occurs when the released material is a superheated liquid [3]. The tendency of a material to exhibit aerosolization is not unique to HF, but also occurs for other chemicals as well. This aerosolization tendency can be significantly reduced by introducing an additive which reduces the vapor pressure thereby eliminating flash atomization.

* Corresponding author.

SSDI 0304-3894(95)00053-4

The identification of an appropriate additive for HF as well as novel HF mitigation strategies is facilitated by a theoretical understanding of the release phenomenon. A few release models have been developed to understand the evaporation of droplets in jets [3–5]. The model of Papadourakis et al. [4] consider the evaporation of a single-component drop in a two-phase jet entraining ambient air. Woodward and Papadourakis [5] extend this model by calculating jet trajectories. The rainout (or capture) of the contaminant is determined as the fraction of the initial contaminant mass retained in the drops when they strike the ground. Melham and Saini [3] have formulated the problem of multicomponent releases. In their work, the authors have assumed that the liquid droplets and entrained air in the two-phase jet are in equilibrium. In the work presented here, we have determined that this assumption is not adequate for HF additive releases. Finally, it must be noted that experimental validation of release models has been largely restricted to monocomponent superheated releases.

In this paper, we build on the previous studies and develop a model formulation for multicomponent releases, without restricting the drops in the jet to be in equilibrium with the entrained air. Applications to multicomponent subcooled HF/additive systems are considered and effects of HF vapor-phase oligomerization, HF–water complexation and aerosol formation are included. The objective of this work is to be able to interpret HF/additive release data and to derive an understanding of aerosol behavior of HF/additive mixtures. The outline of this paper is as follows: Section 2 presents the physical premises and the mathematical formulation of the model; Section 3 is used to interpret small and large-scale HF/additive release test data using the model; Section 4 describes a parametric study of the model predictions; a limiting equilibrium solution which can be viewed as a lower bound on HF rainout is described in Section 5; finally, the principal conclusions of this work are summarized in Section 6.

2. Physical and mathematical description of the model

This section describes the salient physical features and principal assumptions of the model. The general description of droplet evaporation is presented in Section 2.1. A high-pressure liquid issuing from the orifice entrains air and expands to form a two-phase jet (vapor or fog and liquid). Prior to discussing the two-phase jet model, we describe the evaporation of an isolated, multicomponent moving drop in air in Section 2.2. The difference between isolated drop evaporation and evaporation in a two-phase jet is depicted in Fig. 1. In the former case, the drop is surrounded by ambient air and hence the driving force for evaporation is very high. In the latter case, the drop is surrounded by a vapor–liquid fog which contains HF and this reduces the driving force for HF evaporation from the drops. Fig. 1 is again discussed in Sections 2.2 and 2.3 in the setting of the isolated drop and two-phase jet models. The isolated drop model is devoid of the complications arising from air entrainment effects present in the two-phase jet model and is expected to yield a lower bound on HF rainout [4]. Section 2.3 is devoted to the description of the two-phase jet model.

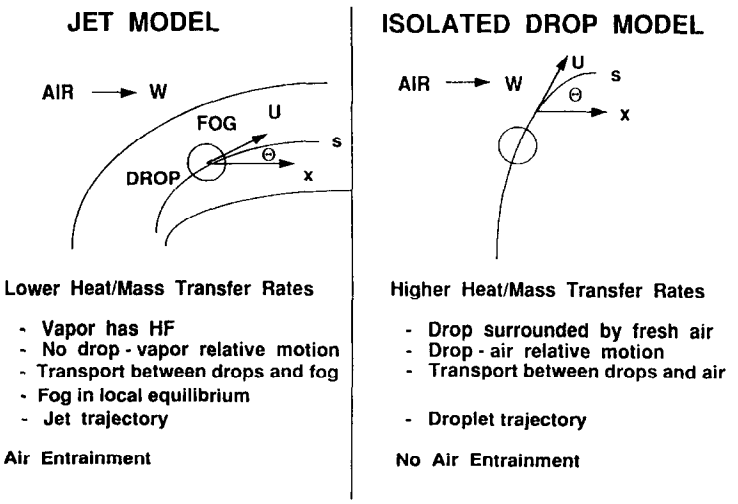

Fig. 1. Jet and isolated drop evaporation.

2.1. Description of drop evaporation

The four species in the system are HF (1), water (2), additive (3) and dry air (4). We develop the equations describing mass and energy exchange for the HF/additive/water system. A rational description of the mass and enthalpy fluxes requires an accurate treatment of HF vapor-phase oligomerization and complexation with water [6] (For example, the heat of vaporization of HF to monomer in vapor is about 7231 cal/g mol at 25 °C whereas the vapor-phase association effects reduce it to about 1700 cal/g mol). HF in vapor is assumed to exist as monomer, dimer, hexamer, octamer and the HF–H_2O complex. Let y_{11}, y_{12}, y_{16}, y_{18} and y_c represent the corresponding vapor mole fractions. The vapor compositions of dry air, additive and water vapor are represented by y_a, y_{add} and y_w, respectively.

We now define the real and apparent mole fractions of HF, additive, water and air. The true mole fractions (y_1, y_2, y_3 and y_4) represent the ratio of the species partial pressures to the total pressure (P) and are given by

$$y_1 = y_{11} + y_{12} + y_{16} + y_{18} + \beta_1 y_c = P_{HF}/P,$$

$$y_2 = y_w + \beta_2 y_c = P_w/P,$$

$$y_3 = y_{add} = P_{add}/P,$$

$$y_4 = y_a = P_a/P.$$

In the above β_1 is the fractional contribution of the HF–H_2O complex to the HF partial pressure and β_2 is its fractional contribution to the partial pressure of water. On making the sum of β_1 and β_2 equal to unity, it is evident that the true mole

fractions satisfy the normalization condition

$$y_1 + y_2 + y_3 + y_4 = 1.$$

The apparent mole fraction (Y_1, Y_2, Y_3 and Y_4) are defined by

$$Y_1 = (y_{11} + 2y_{12} + 6y_{16} + 8y_{18} + y_c)/Q,$$

$$Y_2 = (y_w + y_c)/Q,$$

$$Y_3 = y_{add}/Q,$$

$$Y_4 = y_a/Q,$$

where the normalizing factor is given by

$$Q = y_{11} + 2y_{12} + 6y_{16} + 8y_{18} + 2y_c + y_w + y_{add} + y_a.$$

The factor Q is greater than unity and its deviation from unity measures the extent of vapor-phase oligomerization and HF–water complexation effects. Thus it is unity when this chemistry is absent.

The molar flux of HF (MW = 20.01) to the drops is approximated by

$$F_{HF} = \frac{P}{RT_v}\left[\sum_{i=1,2,6,8} ik_{1i}(y_{1i} - y_{1i}^*) + k_c(y_c - y_c^*)\right],$$

where k_{1i} and k_c denote the mass transfer coefficients for the i-mer and complex, respectively, the superscript $*$ denotes compositions in equilibrium with the liquid at the liquid–vapor interface, T_v is the surrounding temperature and R is the universal gas constant. On assuming equal mass transfer coefficients for the different oligomers and the complex, we have

$$F_{HF} = \frac{P}{RT_v}k_g(QY_1 - Q^*Y_1^*).$$

The above form of the driving force is appropriate when bulk flow is small compared to diffusive flux. In the present situation, bulk flow is expected to be small because HF and water transport in opposite directions. On further assuming equal mass transfer coefficients for all the species, the molar fluxes (F_i, $i = 1, 2, 3, 4$) may be written as

$$F_i = \frac{P}{RT_v}k_g(QY_i - Q^*Y_i^*), \quad i = 1, 2, 3, 4. \tag{2.1}$$

It is possible to proceed with model formulation without making the assumption of equal mass transfer coefficients for all the species. However, given the level of uncertainties and approximations in the overall model, the increased complexity brought about by allowing the species mass transfer coefficients to be different is unwarranted. Moreover, for the additives discussed in this paper and air, there is negligible transport and as such this approximation introduces negligible error. It is, however, easy to account for species-dependent mass transfer coefficients.

We now consider the enthalpy flux. The molar enthalpy (h) of the vapor may be written in terms of those of the individual species as

$$h = \sum_{i=1,2,6,8} y_{1i}h_{1i} + y_c h_c + y_w h_w + y_{add}h_{add} + y_a h_a.$$

The above may be written as

$$h = \left(\sum_{i=1,2,6,8} iy_{1i} + y_c\right)h_{11} + \sum_{i=2,6,8} y_{1i}\Delta H_i + y_c\Delta H_c + (y_w + y_c)h_w + y_{add}h_{add} + y_a h_a,$$

where ΔH_i is the enthalpy of formation of the i-mer (the reaction is $i\mathrm{HF} \rightarrow \mathrm{HF}_i$) and ΔH_c is the enthalpy of formation of the complex (the reaction is $\mathrm{HF} + \mathrm{H_2O} \rightarrow \mathrm{HF \cdot H_2O}$). After some algebraic manipulations, one can derive an expression for apparent molar enthalpy of the vapor, H^a as

$$H^a = h/Q = Y_1(h_{11} + \Delta) + Y_2 h_w + Y_3 h_{add} + Y_4 h_a,$$

where Δ is the enthalpy deviation function defined by

$$\Delta = \frac{y_{12}\Delta H_2 + y_{16}\Delta H_6 + y_{18}\Delta H_8 + y_c\Delta H_c}{y_{11} + 2y_{12} + 6y_{16} + 8y_{18} + y_c}.$$

The enthalpy flux to the drops associated with mass exchange with the vapor can now be written as

$$F_e = \frac{Pk_g}{RT_v}[(QY_1 - Q^*Y_1^*)h_1 + (QY_2 - Q^*Y_2^*)h_w + (QY_3 - Q^*Y_3^*)h_{add}], \quad (2.2)$$

where

$$h_1 = h_{11} + \Delta.$$

For a droplet moving at a velocity U along a trajectory described by a curvilinear coordinate s, we write

$$\frac{d(m_d\omega_i)}{ds} = \pi\frac{D_d^2}{U}\frac{Pk_g}{RT_v}(QY_i - Q^*Y_i^*), \quad i = 1, 2, 3, \quad (2.3)$$

where m_d is the total number of moles in the drop, ω_i is the mole fraction of species i in the drop and D_d is its diameter. The enthalpy balance is given by

$$\frac{d(m_d h_d)}{ds} = \frac{\pi D_d^2}{U}\frac{Pk_g}{RT_v}\left[\sum_{i=1,2,3}(QY_i - Q^*Y_i^*)h_i^*\right] + \frac{\pi D_d^2}{U}h_t(T_v - T_d). \quad (2.4)$$

In the above, h_d is the molar enthalpy of the drop, h_t is the heat transfer coefficient, T_v is the surrounding temperature and T_d is the droplet temperature. The reference state for enthalpy calculations is that of an ideal gas at 25 °C. For HF, the reference state is an ideal monomer vapor at 25 °C.

2.2. Isolated drop evaporation

The physical picture is shown in Fig. 1. The driving force for HF evaporation from the drop is maximum since it is always surrounded by ambient air free of HF. The mathematical model for evaporation of a moving droplet involves a description of heat and mass exchange between the drop and the surrounding as well as droplet dynamics and kinematics [4]. The transport coefficients for mass/heat exchange between the droplets depend on the nature of drop–air relative motion and as such the drop motion and transport processes are coupled. The vapor-phase concentrations away from the drop are the same as those of ambient air. Thus, since ambient air is free of HF or additive, we have

$$Y_1 = Y_3 = 0, \qquad Q = 1, \qquad Y_2 = y_w^0, \qquad Y_4 = y_a^0, \tag{2.5}$$

where y_w^0 and y_a^0 are the mole fractions of water vapor and dry air in ambient air. These are determined from the air temperature (T^0) and the relative humidity. We are now ready to write the drop mass and energy balances. We assume no transport of dry air between the two phases. Thus HF, additive and water are the components of interest.

Component mass balances

Using Eq. (2.3) and the above approximation, we obtain

$$\frac{d(m_d\omega_i)}{ds} = \frac{\pi D_d^2}{U}\frac{Pk_g}{RT^0}(-Q^*Y_i^*), \quad i = 1,3, \tag{2.6}$$

$$\frac{d(m_d\omega_2)}{ds} = \frac{\pi D_d^2}{U}\frac{Pk_g}{RT^0}(y_w^0 - Q^*Y_2^*).$$

The mass transfer coefficient (k_g) is obtained from an empirical correlation relating the drop Sherwood number (Sh) to the Reynolds number (Re) and the Schmidt number (Sc). This correlation is given by [4]

$$Sh = \alpha + \beta Re^{1/2}Sc^{1/3}, \quad \alpha = 2, \quad \beta = 0.6. \tag{2.7}$$

In the above, the Reynolds number is defined by

$$Re = \frac{D_d U_{dr}\rho_a}{\mu_a}, \tag{2.8}$$

where μ_a is the dynamic viscosity of air. The Sherwood (Sh) and Schmidt (Sc) numbers are given by

$$Sh = \frac{k_g D_d}{D}, \qquad Sc = \frac{\mu_a}{\rho_a D} \tag{2.9}$$

where D is the binary diffusivity taken as $2.2 \times 10^{-5}\ m^2\,s^{-1}$ for all the species.

Energy balance

From Eqs. (2.4) and (2.5) one gets

$$\frac{\mathrm{d}(m_\mathrm{d}h_\mathrm{d})}{\mathrm{d}s} = \frac{\pi D_\mathrm{d}^2}{U}\frac{Pk_\mathrm{g}}{RT^0}\left[\sum_{i=1,3}(-Q^*Y_i^*)h_i^* + (y_\mathrm{w}^0 - Q^*Y_2^*)h_2^*\right] + \frac{\pi D_\mathrm{d}^2}{U}h_\mathrm{t}(T^0 - T_\mathrm{d}), \tag{2.10}$$

where the enthalpies are evaluated at the droplet temperature (T_d). The heat transfer coefficient is obtained from

$$N = \alpha + \beta Re^{1/2}Pr^{1/3}, \quad \alpha = 2, \quad \beta = 0.6, \tag{2.11}$$

where the Nusselt number (Nu) and the Prandtl number (Pr) are given by

$$Nu = \frac{h_\mathrm{t}D_\mathrm{d}}{k_\mathrm{a}}, \qquad Pr = \frac{\mathrm{Cp_a}\mu_\mathrm{a}}{k_\mathrm{a}\mathrm{MW_a}}, \tag{2.12}$$

In the above, $\mathrm{Cp_a}$, k_a and $\mathrm{MW_a}$ are the molar heat capacity, thermal conductivity and molecular weight of air, respectively.

The droplet trajectory in air is determined using momentum balances.

Drop momentum balances

Assuming that mass exchange between the drop and the vapor takes place at negligible velocity with respect to the drop (no thrust on the drop), and letting U_dx and U_dy denote the x (horizontal) and y (vertical) velocities of the drops (with respect to a fixed frame of reference), we have

$$\frac{\mathrm{d}(m_\mathrm{d}U_\mathrm{dx})}{\mathrm{d}t} = U_\mathrm{dx}\frac{\mathrm{d}m_\mathrm{d}}{\mathrm{d}t} + F_x,$$

where the first term on the right-hand side represents the momentum change due to mass transfer and the second accounts for the effect of external forces, namely drag on the drop. On noting that

$$\frac{\mathrm{d}s}{\mathrm{d}t} = U$$

one obtains

$$m_\mathrm{d}\frac{\mathrm{d}U_\mathrm{dx}}{\mathrm{d}s} = F_x/U,$$

where F_x is the horizontal drag on the drop and is given by

$$F_x = -C_\mathrm{d}(1/4\pi D_\mathrm{d}^2)(1/2\rho_\mathrm{a}U_\mathrm{dxr}U_\mathrm{dr}).$$

In the above, C_d is the drag coefficient and the drop–air relative velocities are given by

$$U_\mathrm{dxr} = U_\mathrm{dx} - w, \qquad U_\mathrm{dyr} = U_\mathrm{dy}, \qquad U_\mathrm{dr}^2 = U_\mathrm{2dxr} + U_\mathrm{dyr}^2,$$

where w is the component of the wind speed in the x direction. Combining these,

$$\frac{dU_{dx}}{ds} = -\frac{C_d(\pi D_d^2/4)(1/2\rho_a U_{dxr} U_{dr})}{m_d U}, \tag{2.13}$$

where U is the drop speed and s is distance along the curvilinear trajectory (Fig. 1). The momentum balance along the y (vertical) direction yields

$$\frac{dU_{dy}}{ds} = -\frac{[C_d(\pi D_d^2/4)(1/2\rho_a U_{dyr} U_{dr}) + (1 - \rho_a/\rho_d) g m_d]}{m_d U}. \tag{2.14}$$

The first term on the right-hand side represents drag and the second term accounts for gravity and buoyancy forces. The drag coefficient appearing in the momentum balances is a function of the Reynolds number for drop–air relative motion. The drag coefficient is given by [7]

$$C_d = 24/Re, \quad Re < 0.1,$$

$$C_d = (24/Re)(1 + 3Re/16 + 9Re^2 \ln(2Re)/160), \quad 0.1 < Re < 2,$$

$$C_d = (24/Re)(1 + 0.15Re^{0.687}), \quad 2 < Re < 500,$$

$$C_d = 0.44, \quad 500 < Re < 200{,}000. \tag{2.15}$$

The drop trajectory calculations are completed along with a description of the kinematics of motion

$$\frac{dx_d}{ds} = \frac{U_{dx}}{U}, \qquad \frac{dy_d}{ds} = \frac{U_{dy}}{U}. \tag{2.16}$$

Fig. 2 describes the effect of drop size on HF capture. HF rainout (or capture) is defined as the fraction of initial HF that is retained in the drop when it strikes the ground. The rainout decreases with decreasing droplet size and is very sensitive to size as the size decreases. This is because the specific surface area (area per unit mass) increases (as 1/diameter) and this leads to faster HF evaporation.

Fig. 3(a) depicts typical droplet trajectories. The larger droplets, owing to their higher inertia, travel farther before striking the ground. Fig. 3(b) shows the fraction of initial HF, additive and water retained in the drops (right y axis) as well as the droplet temperature along its trajectory (left y axis). The HF evaporation rates appear to decrease along the trajectory. This is because of two reasons. First the decreasing speed of the droplets decreases the mass and heat transfer coefficients. Second, the vapor pressure rapidly decreases due to HF evaporation and the accompanying cooling. The nonvolatile additive is almost entirely in the drops. The increase of water in the drops is also evident. The droplet temperature first decreases rapidly as HF evaporation dominates water condensation into the drops. After substantial HF has evaporated, the heating accompanying water condensation into the drops more than offsets the cooling due to HF evaporation and the drop temperature begins to rise again. Such a phenomenon would not be observed in models that do not allow for water condensation.

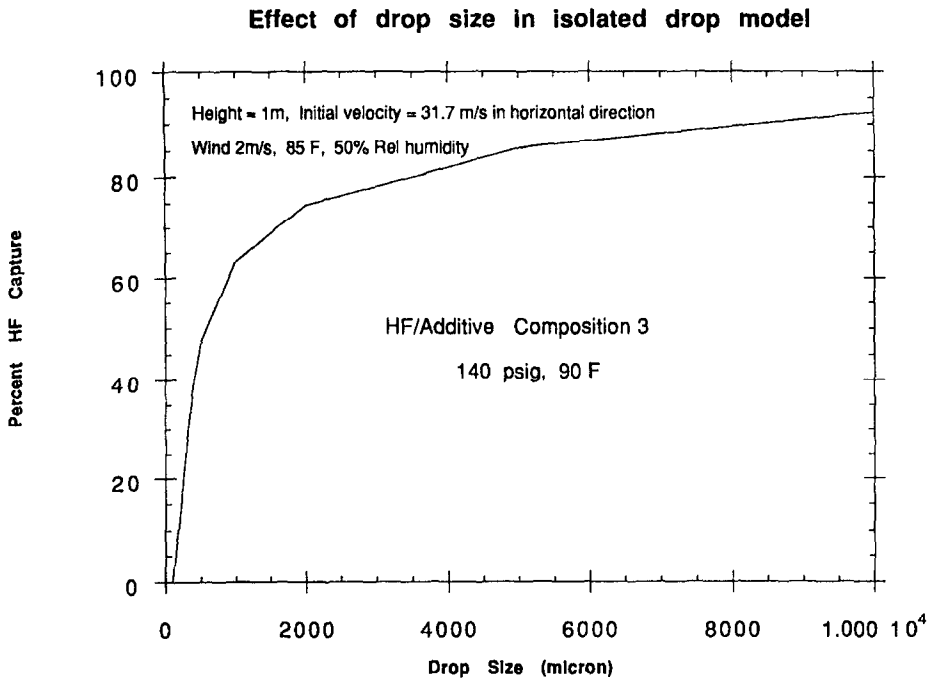

Fig. 2. Effect of drop size in isolated drop model.

2.3. *Two-phase jet model*

In this section, we highlight the principal physical features of the two-phase jet model. Fig. 1 shows the geometry and coordinates and Fig. 4 depicts the different mechanisms that are featured in the model. As the jet comes out of the orifice, it expands by entraining ambient air [8]. Flashing jets (above critical superheat) additionally expand by instantaneously equilibrating partly into vapor. This process, referred to as flash atomization, can also potentially break the jet into very small liquid droplets. In what follows, we will restrict to situations where such flash atomization does not occur. The HF evaporating from the drops interacts with the entrained air to form a vapor–liquid fog. The drops of the release stream along with the fog constitute a two-phase jet. In contrast to the isolated drop (described in the previous section), which is surrounded by HF-free air, a droplet inside a two-phase jet is surrounded by a vapor–liquid fog that has HF. Therefore, a drop inside a two-phase jet experiences a smaller driving force for HF evaporation than an isolated drop. The model is constructed with the following assumptions:

1. In the immediate vicinity of the orifice, the jet may consist of an intact liquid core. Any evaporation in this region is neglected owing to the small specific surface area available.

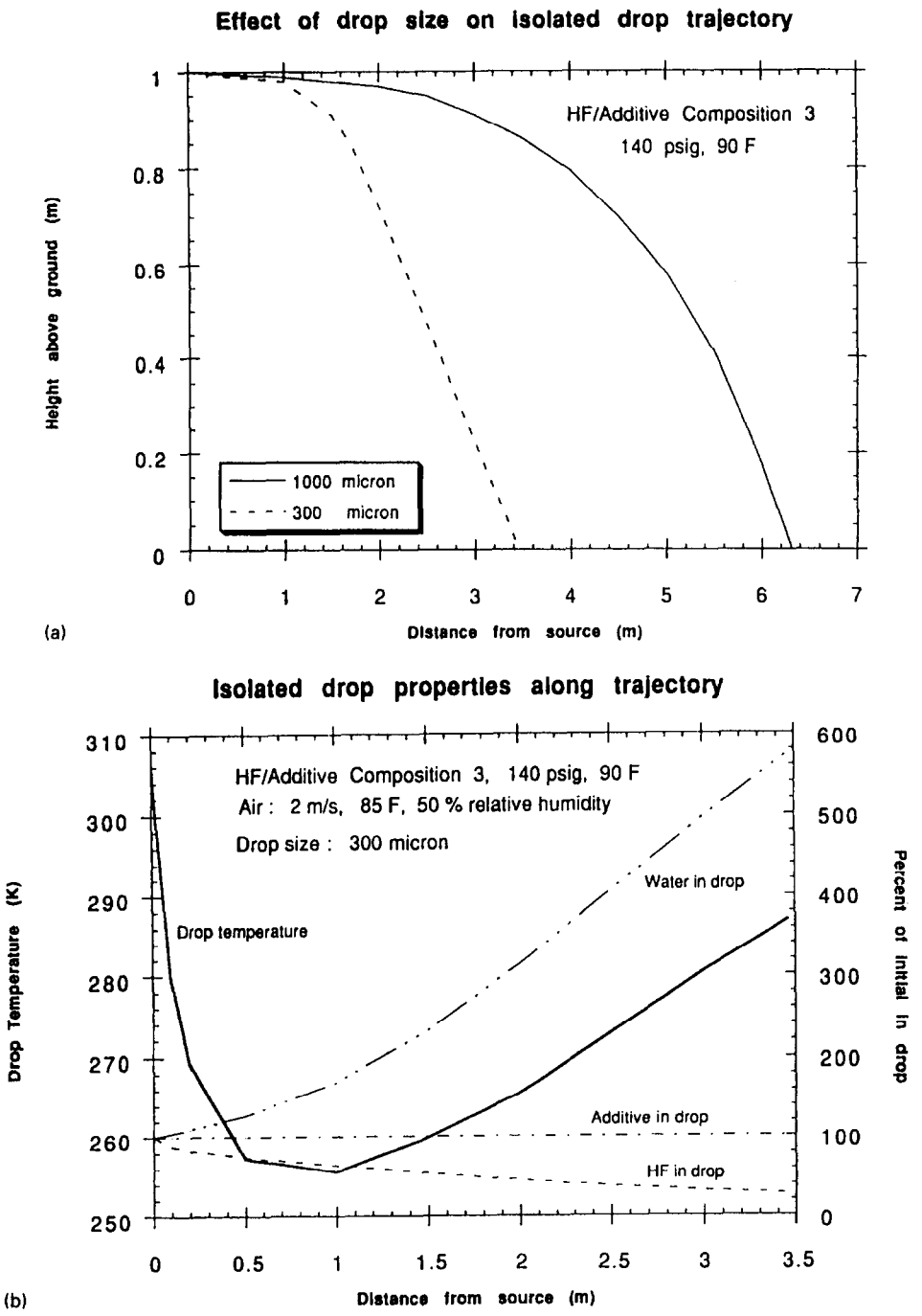

Fig. 3. (a) Effect of drop size on isolated drop trajectory. (b) Isolated drop properties along trajectory.

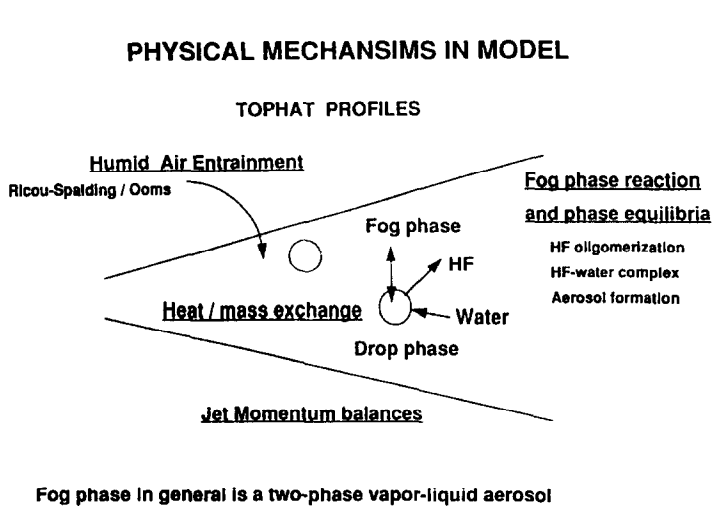

Fig. 4. Physical mechansims in model.

2. At the end of the intact region, the liquid core is assumed to instantaneously rupture into droplets (parent drops) producing a two-phase mixture with a volume fraction of drops ε_{p0}. Air entrainment such as described by Ricou and Spalding [8] and Ooms [9] commences at the end of the intact region and causes the jet to expand. The mixture velocity at the end of the intact region and the beginning of the entrainment zone is assumed to be the same as the jet velocity at the orifice. The phase surrounding these parent drops in the jet is in general a vapor–liquid fog.

3. In general, the droplets of various diameters will be formed upon rupture of the jet. Therefore, a rigorous model should account for this drop size distribution. However, as a simplification, we will assume that the essential physics can be captured by a single characteristic drop size. Since mass and heat transfer are the phenomena of interest, this characteristic drop size is identified as the Sauter mean diameter.

4. The parent drops are in general not in equilibrium with the surrounding fog and exchange mass and energy with the vapor in the jet. Thus the drops are in general at a different temperature than the fog.

5. Multicomponent diffusivities in the vapor are approximated with binary diffusivities of species in air. Equal diffusivities are assumed for HF and its oligomers and water.

6. The HF evaporating from the drops interacts with entrained humid air to form a fog (vapor + liquid) [6]. The fog properties at any axial location are determined from local equilibrium assumption. Thus the vapor in the jet is actually a fog (vapor + liquid particles).

7. The fog equilibrium is calculated accounting for HF vapor-phase oligomerization, HF–water complexation as well as HF/additive/water vapor–liquid equilibria.

8. There is no relative motion between the drops and the surrounding fog. The jet trajectory is calculated via jet momentum balances assuming that the jet is

pseudo-homogeneous. In other words, the drops are always inside the jet and the jet itself is well mixed in a plane perpendicular to the jet axis. The assumption of drops being inside the jet is expected to be good for high momentum releases that are of interest in this paper.

9. Given the initial release conditions, the jet trajectory is tracked until the centerline hits the ground. The rainout of HF is defined as the fraction of released HF that is retained in the parent drops. Thus the HF in the fog (vapor + liquid) is assumed to be airborne. This is a reasonable assumption since the aerosol particles are expected to be in the upper Brownian size scale and to remain suspended in vapor.

10. The vapor pressures of HF, additive and water at a given liquid composition and temperature can be predicted using a liquid-phase activity coefficient model. For the particular additive discussed in this paper, the NRTL model (Appendix A) was found to be adequate. Each of the species in the vapor phase (HF and its oligomers, HF–water complex, water, additive and dry air) is assumed to behave ideally. We now present a mathematical formulation of the two-phase jet.

Transition from intact to two-phase jet/jet initialization

The jet is assumed to rupture immediately after the intact zone and any effect of the intact zone is neglected. This requires that the time scale up to jet rupture be much smaller than the time of flight of the jet. Some air is also assumed to be entrained to form a two-phase jet. The drops are assumed to be of the same composition and temperature as that of the liquid just before the orifice. The two-phase jet is assumed to have the velocity of the release stream issuing out of the orifice. The jet centerline is described by the coordinate s and the jet angle with respect to the horizontal is given by θ (Fig. 1).

The two-phase jet variables are its radius (R_{TP}), velocity components (U_{TPX} and U_{TPY}), coordinates of jet centerline (X_{TP}, Y_{TP}), drop volume fraction (ε_p), drop compositions (ω_i, $i = 1, 2, 3$), drop temperature (T_d), fog liquid volume fraction (f_l), fog vapor and fog liquid compositions and fog temperature (T_f). In view of the above assumptions, the following initializations serve to describe the net effects of the transition region:

$$\omega_i(0+) = \omega_i(0-),$$

$$T_d(0+) = T(0-) = \text{release temperature},$$

$$U_{TPX}(0+) = u_0 \cos\theta, \qquad U_{TPY}(0+) = u_0 \sin\theta,$$

$$X_{TP}(0+) = X(0-), \qquad Y_{TP}(0+) = Y(0-),$$

$$T_f(0_+) = T^0,$$

$$f_l(0+) = 0,$$

where $s = 0-$ refers to conditions just upstream of the orifice and $s = 0+$ pertains to conditions at the onset of the entrainment region. The initial fog vapor composition is assumed to be that of ambient air. In order to complete the characterization of the two-phase jet, the parent drop volume fraction at $0+$ ε_{p0}, must be specified as an

input parameter. Conservation of the release material volumetric flow rate across the transition region and the assumption of no change in velocity requires that the jet radius be given by

$$R_{TP}(0+) = [D_j^2/(4\varepsilon_{p0})]^{0.5}.$$

The initial two-phase density is given by

$$\rho_{TP}(0+) = \varepsilon_{p0}\rho_l + (1 - \varepsilon_{p0})\rho_a,$$

where ρ_l is the density of the liquid exiting the orifice. The initial drop size (D_{d0}) is another important input parameter. Alternatively, it may be determined using a suitable criterion. Typically, a Weber number approach [3–5] is employed.

Air entrainment by two-phase jet

The two-phase jet expands by entraining ambient air [8, 9]. We assume top-hat profiles (no variation of properties across jet cross section). In general, the entrainment is regarded as a sum of three contributions and the specific rate of entrainment of humid air is described by [9]

$$\frac{dm_a}{ds} = 2\pi R_{TP}\rho_a\left\{\alpha_1\sqrt{\frac{\rho_{TP}}{\rho_a}}|U_{TP} - w\cos\theta| + \alpha_2|\sin\theta|\cos\theta w + \alpha_3 u'\right\} \tag{2.17a}$$

with the entrainment coefficients chosen as

$$\alpha_1 = 0.0806, \qquad \alpha_2 = 0.5, \qquad \alpha_3 = 1.0. \tag{2.17b}$$

In the above, ρ_{TP} is the two-phase jet density (see Eq. (2.26)).

The first contribution to entrainment in Eq. (2.17a), referred to as free jet entrainment, is dominant when the jet velocity is much greater than that of wind. The coefficient α_1 has been chosen to match the experimentally established entrainment rates of Ricou and Spalding [8]. When the velocity of the jet becomes comparable to that of air, entrainment is described as that of a cylindrical thermal plume in a stagnant atmosphere and this represents the second contribution to entrainment. The last contribution comes from atmospheric turbulence and u' is the root mean squared velocity fluctuation for turbulent flow. It may be approximated by

$$u' = (\varepsilon R_{TP})^{1/3}, \tag{2.17c}$$

where ε is the turbulence energy dissipation per unit mass and is given by

$$\varepsilon = 0.0677\, w/y$$

for a neutral atmosphere [10]. Kaimal et al. [11] assign ε values of 0.004 and 0.0 for unstable and stable atmospheres, respectively. The chosen values for the entrainment coefficients α_2 and α_3 have been suggested by Ooms [9]. When only the first contribution to entrainment is considered, the model reduces to that of Ricou and Spalding [8].

We can now write the drop and jet mass and energy balances. The molar rate of entrainment of water vapor and dry air are readily identified as

$$\frac{dz_i}{ds} = \frac{dm_a}{ds}\frac{Py_i^0}{RT^0\rho_a}, \qquad i = 2, 4. \tag{2.18}$$

Parent drop component material balances

HF, additive and water are the three transferring species. The drops in this case, exchange mass with the fog phase. Thus, the material balances are obtained from Eq. (2.3) with the bulk phase concentrations set equal to the fog vapor compositions. Thus

$$\frac{d(m_d\omega_i)}{ds} = \frac{\pi D_d^2}{U_{TP}}\frac{Pk_g}{RT_f}(Q^f Y_i^f - Q^* Y_i^*), \quad i = 1, 2, 3, \tag{2.19}$$

where the superscript, f, is used to denote quantities pertaining to the fog.

Parent drop enthalpy balance

Denoting the molar enthalpy of the drop by h_d, we have,

$$\frac{d(m_d h_d)}{ds} = \frac{\pi D_d^2}{U_{TP}}\frac{Pk_g}{RT_f}\left[\sum_{i=1,2,3}(Q^f Y_i^f - Q^* Y_i^*)h_i^*\right] + \frac{\pi D_d^2}{U_{TP}}h_t(T_f - T_d). \tag{2.20}$$

Unlike in the case of evaporation of an isolated drop, there is no relative motion between the drops and the surrounding fog in the two-phase jet. Hence the mass and heat transfer coefficients are obtained by setting the Sherwood and Nusselt numbers equal to 2. Thus,

$$Sh = \frac{k_g D_d}{D} = 2, \qquad Nu = \frac{h_t D_d}{k_f} = 2,$$

where k_f is the thermal conductivity of the fog and is approximated with the value of air (k_a).

Fog phase component material balances

Let $\zeta_i(s)$, $i = 1, \ldots, 4$, denote the molar flow rates of HF, water, additive and dry air in the fog (HF based on molecular weight of 20.01). Part of this is associated with the fog liquid and the remaining with fog vapor. The component material balances may be written as

$$\frac{d\zeta_i}{ds} = -N_d\frac{\pi D_d^2}{U_{TP}}\frac{Pk_g}{RT_f}(Q^f Y_i^f - Q^* Y_i^*), \qquad i = 1, 3, \tag{2.21a}$$

where N_d is the number flow rate of drops (a constant) and is given by

$$N_d = \frac{\pi R_{TP}^2 U_{TP}\varepsilon_p}{\pi D_d^3/6}.$$

In the case of water, the mass balance should also account for moisture brought into the fog phase by air entrainment. Thus it takes the form

$$\frac{d\zeta_2}{ds} = -N_d \frac{\pi D_d^2}{U_{TP}} \frac{Pk_g}{RT_f}(Q^f Y_2^f - Q^* Y_2^*) + \frac{dz_2}{ds}. \tag{2.21b}$$

In the case of dry air, there is no mass exchange with the parent drops so that the differential material balance is given by

$$\frac{d\zeta_4}{ds} = \frac{dz_4}{ds}. \tag{2.21c}$$

Fog phase enthalpy balance

The enthalpy of the fog phase changes due to mass exchange with the parent drop phase, heat transfer with the parent drops and humid air entrainment. The total fog enthalpy, ψ, satisfies the conservation law

$$\frac{d\psi}{ds} = -N_d \left\{ \frac{\pi D_d^2}{U_{TP}} \frac{Pk_g}{RT_f} \left[\sum_{i=1,2,3} (Q^f Y_i^f - Q^* Y_i^*) h_i^* \right] + \frac{\pi D_d^2}{U_{TP}} h_t (T_f - T_d) \right\} + h_2^0 \frac{dz_2}{ds} + h_4^0 \frac{dz_4}{ds}. \tag{2.22}$$

Once the mass and enthalpy flow rates in the fog are known, the fog temperature, fog liquid volume fraction and vapor/liquid compositions may be obtained by consideration of local equilibrium at s (Appendix A).

Jet momentum balances

The calculation of the jet trajectory requires the use of momentum balances. Let p_x and p_y denote the components of the jet momentum flux along the horizontal and vertical directions. These are given by

$$p_x = \pi R_{TP}^2 \rho_{TP} U_{TP}^2 \cos\theta, \qquad p_y = \pi R_{TP}^2 \rho_{TP} U_{TP}^2 \sin\theta.$$

The horizontal component obeys the conservation law [9]

$$\frac{dp_x}{ds} = w \frac{dm_a}{ds} + C_d \pi R_{TP} \rho_a w^2 |\sin^3\theta|, \tag{2.23}$$

where the first term describes the increase of momentum accompanying the entrainment of air and the second describes an increase in impulse due to drag force exerted on the plume by the wind. The y component momentum balance is given by

$$\frac{dp_y}{ds} = \pi R_{TP}^2 g(\rho_a - \rho_{TP}) \pm C_d \pi R_{TP} \rho_a w^2 \cos\theta \sin\theta |\sin\theta|, \tag{2.24}$$

where the first term accounts for gravity and buoyancy and the second represents a drag term. The value of C_d is 0.3. The $+$ sign is valid for $-\pi/2 \leqslant \theta < 0$ and the

– sign for $0 \leqslant \theta < \pi/2$. The jet trajectory is computed from the kinematic equations

$$\frac{dX_i}{ds} = \cos\theta, \qquad \frac{dY_i}{ds} = \sin\theta. \tag{2.25}$$

Two-phase jet characteristics

We now develop the necessary relationships to determine the jet radius (R_{TP}), jet speed (U_{TP}), overall jet density (ρ_{TP}), parent drop volume fraction (ε_p) and jet angle (θ). The two-phase density is defined by

$$\rho_{TP} = \varepsilon_p \rho_d + (1 - \varepsilon_p)[\rho_{fv}(1 - f_l) + f_l \rho_{fl}], \tag{2.26}$$

where the fog densities ρ_{fv} and ρ_{fl} and the fog liquid volume fraction, f_l, are obtained from the solution of the fog equilibrium problem. This solution also yields the volumetric flow rate of the fog, v_f, which is related to the jet properties by

$$R_{TP}^2 U_{TP}(1 - \varepsilon_p) = v_f/\pi \equiv \gamma_4. \tag{2.27}$$

Since the drops are always inside the jet, conservation of drop number (N_d) is expressed by

$$R_{TP}^2 U_{TP} \varepsilon_p = \frac{R_{TP}^2(0+) u_0 \varepsilon_{p0} D_d^3}{D_{d0}^3} \equiv \gamma_3. \tag{2.28}$$

The momentum flux along the jet axis is given by

$$\pi R_{TP}^2 \rho_{TP} U_{TP}^2 = \sqrt{p_x^2 + p_y^2} \equiv \pi \gamma_2. \tag{2.29}$$

The jet angle, θ, is readily obtained from

$$\sin\theta = \frac{p_y}{\pi R_{TP}^2 \rho_{TP} U_{TP}^2}. \tag{2.30}$$

The other quantities are readily obtained as

$$\varepsilon_p = \frac{\gamma_3}{\gamma_3 + \gamma_4},$$

$$\rho_{TP} = \frac{1}{\gamma_3 + \gamma_4}\{\gamma_3 \rho_d + \gamma_4[f_l \rho_{fl} + (1 - f_l)\rho_{fv}]\},$$

$$U_{TP} = \gamma_2/[\gamma_3 \rho_d + \gamma_4\{f_l \rho_{fl} + (1 - f_l)\rho_{pv}\}],$$

$$R_{TP}^2 = (\gamma_3 + \gamma_4)[\gamma_3 \rho_d + \gamma_4\{f_l \rho_{fl} + (1 - f_l)\rho_{fv}\}]/\gamma_2.$$

The model solution is obtained by integrating equations (2.19)–(2.25) (with air entrainment described by Eqs (2.17) and (2.18)) for the drop composition and temperature, fog phase material species and enthalpy flow rates as well as the jet moments and position. The fog volumetric flow rates and fog vapor and liquid compositions and fog liquid volume fraction and temperature are obtained as described in Appendix A. The two-phase jet properties are obtained from Eqs. (2.26)–(2.30).

Fig. 5(a) depicts predicted jet centerline trajectories for typical 50, 100 and 140 psig releases for a 0.5 in orifice. As expected, increasing release pressure increases the distance at which the jet centerline strikes the ground. Although the release velocity is roughly proportional to the square root of the release pressure, the rainout distance shows a weaker dependence on pressure because, air entrainment slows the jet along its trajectory. The radius and velocity of an expanding jet (140 psig) along its trajectory are shown in Fig. 5(b). Fig. 5(c) shows the fog temperature, droplet temperature and fraction of initial HF in the drops along the jet trajectory. The drop cools first due to the cooling accompanying HF evaporation exceeding the heating effects of water condensation into the drops. Eventually the drop temperature begins to rise as the enthalpic effects of water condensation dominate over those of HF evaporation. The condensation involved in aerosol formation heats the vapor to above ambient temperature.

3. Model evaluation using release test data

A key parameter in the model is the initial drop size. In this section, we evaluate the model in conjunction with different strategies for estimating the initial characteristic drop size in the jet. Since the applications discussed in this paper are on subcooled releases, the drop size is determined by hydrodynamic breakage. Large scale HF/additive release tests were performed in a flow chamber of Quest Consultants near Norman, Oklahoma [12, 13]. The effect of release mix composition, release mix temperature, storage pressure (50–225 psig) and orifice size (0.125–0.75 in) were studied. Essentially, three modified HF catalyst compositions were studied. Composition 1 had the lowest vapor pressure and Composition 3 had the highest vapor pressure at a given temperature. Section 3.1 is devoted to assessing the overall representation of the large-scale test data. Different strategies for the choice of a characteristic drop size are evaluated. Section 3.2 interprets the effects of different variables observed in the release tests using the model. The model predictions are compared with laboratory scale experiments in Section 3.3.

3.1. Fit of quest HF/additive large scale test data

The model has essentially two parameters, the initial parent drop volume fraction (ε_{p0}) and the initial drop size (D_{d0}). We found that the HF capture is not sensitive over a wide range of the initial drop volume fraction. However, the drop size is a sensitive parameter. The model requires as input the initial characteristic drop size to commence the two-phase jet calculations. Since there appears to be no data to test the individual aspects of the model, only an overall assessment can be made using HF capture data. The initial drop size is expected to depend on surface tension and the release velocity. As there exists no definitive analysis of drop size for atomization, different strategies for estimating the drop size are evaluated on their ability to predict HF capture.

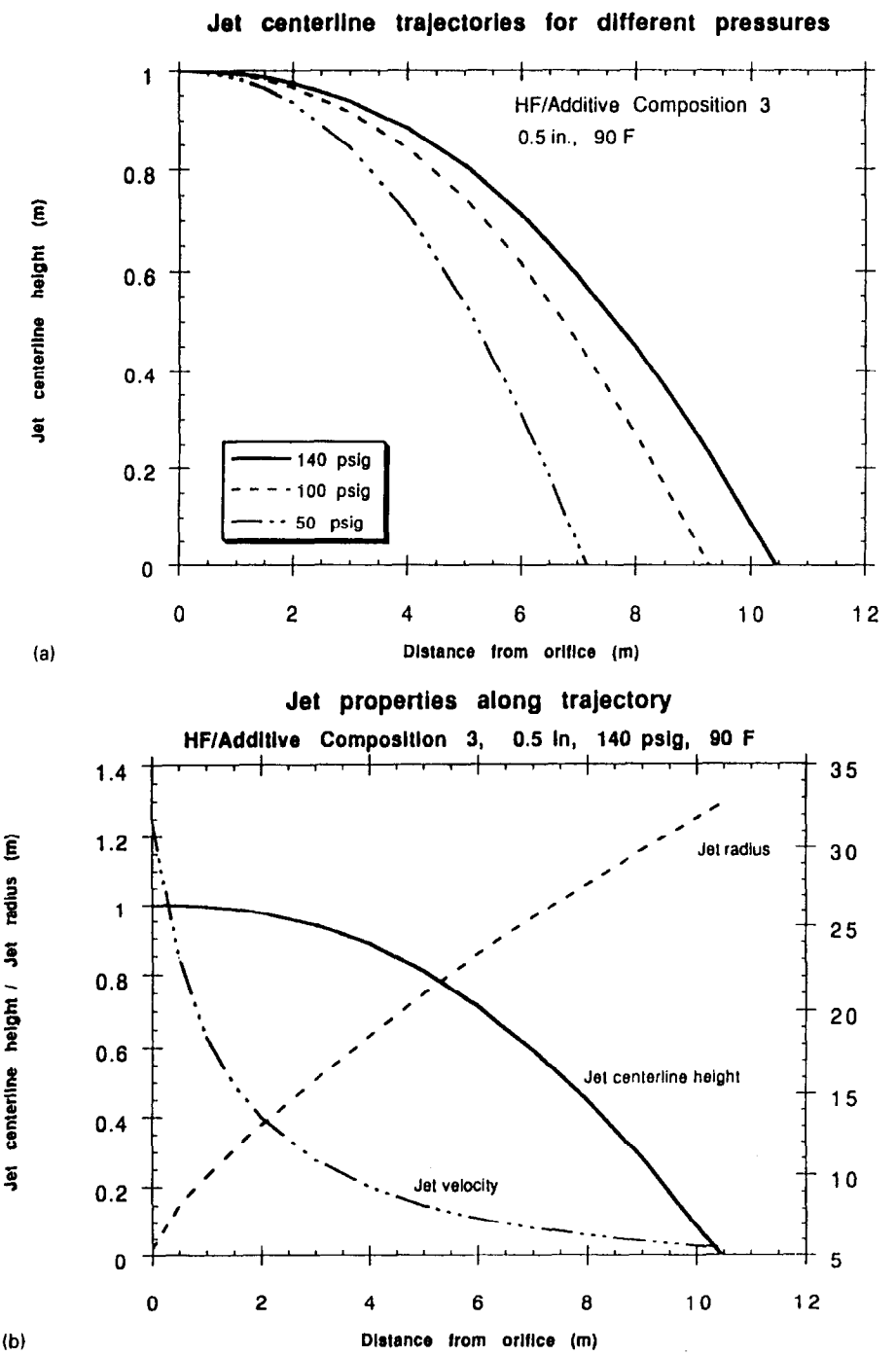

Fig. 5. (a) Jet centerline trajectories for different pressures. (b) Jet properties along trajectory. (c) Drop properties in a two-phase jet.

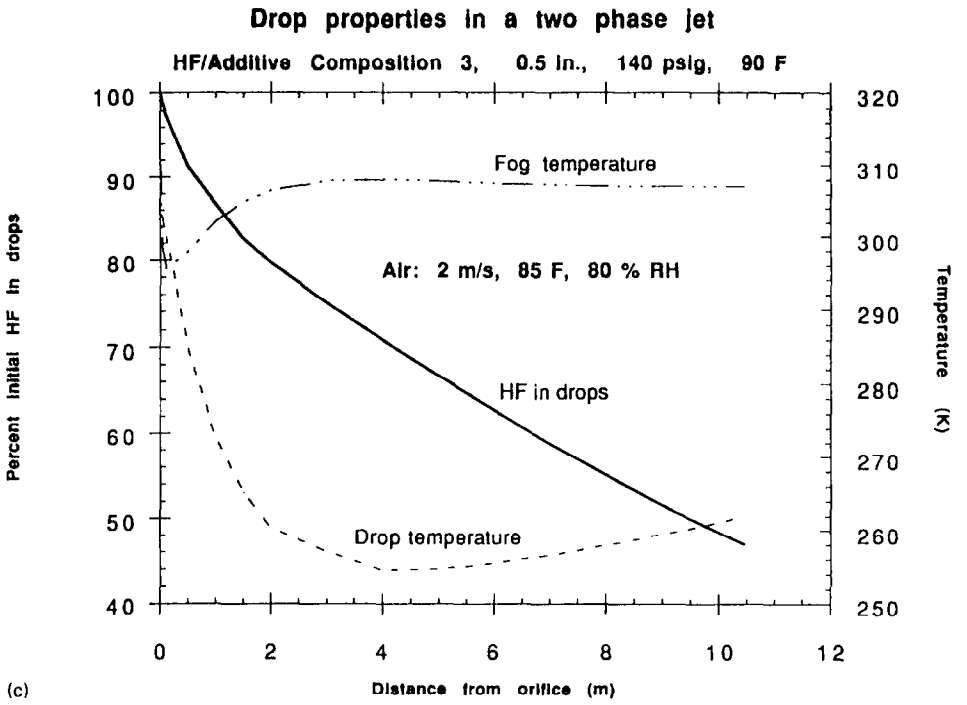

Fig. 5. Continued.

Experimentally measured mass release rate, liquid composition, release vessel temperature, orifice diameter, ambient air properties (temperature and relative humidity) and air speed through the flow chamber were used to initialize the model calculations. The Ricou–Spalding model [8] was used for calculating air entrainment. The height of the orifice from the pans was 1 m and the releases were all horizontal (angle of release = 0°).

Constant drop size

As a first approximation, the initial drop size was assumed to be the same for all the tests. Fig. 6(a) shows the model predictions for HF rainout plotted against the measured values using a drop size of 300 μ. The legend only shows the variables that were held constant. Other conditions could vary. Thus, for example, the different tests with the legend 50 psig, composition 2, had different orifice diameters. Hence we observe varying captures. It is evident that there is good agreement except for Composition 1 (lowest HF vapor pressure) releases. The average absolute deviation, defined as the mean over all cases of the absolute value difference between the model prediction and measured capture, is 5.6. The lack of agreement in the first situation could be due to two reasons. The drop sizes at these compositions could be much

higher due to the significantly higher surface tension. The NRTL model predictions of vapor pressures at these compositions may be inaccurate because the compositions are substantially outside the range of those used to derive the NRTL parameters (Compositions 2 and 3).

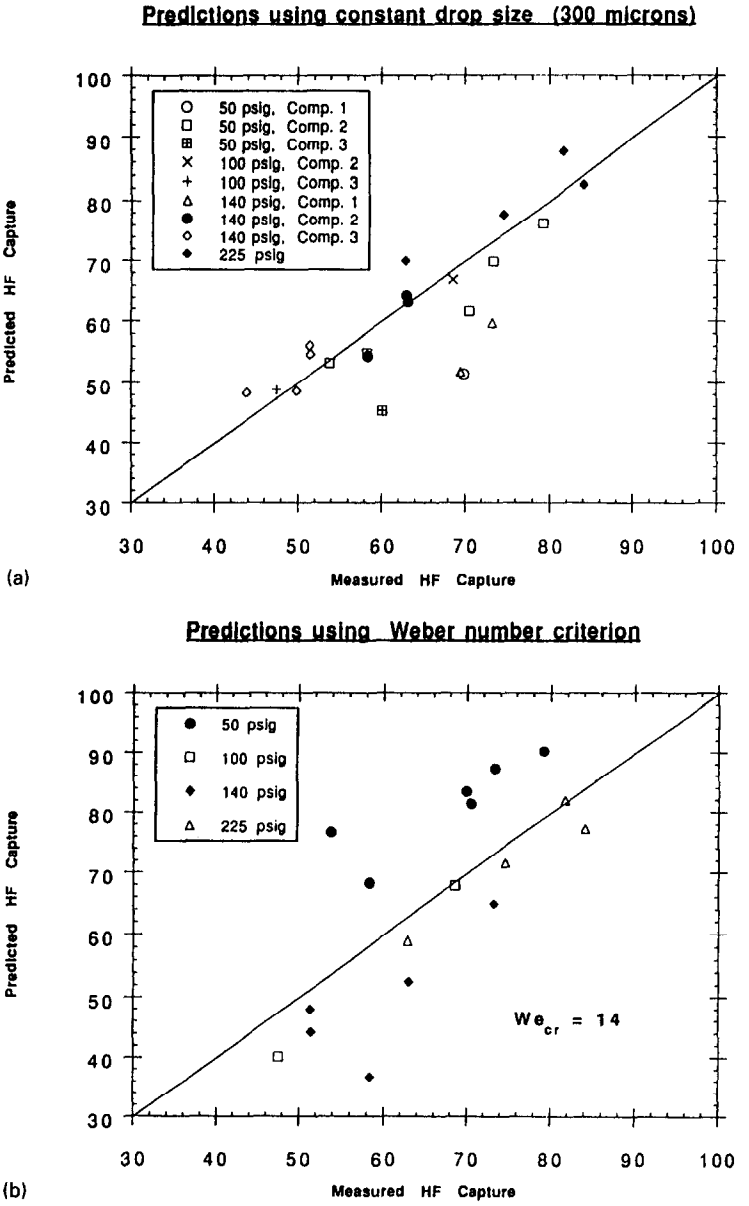

Fig. 6. (a) Predictions using constant drop size (300 microns). (b) Predictions using Weber number criterion. (c) Predictions using modified Weber number criterion. (d) Predictions using $D_d = 0.96\sigma/u$.

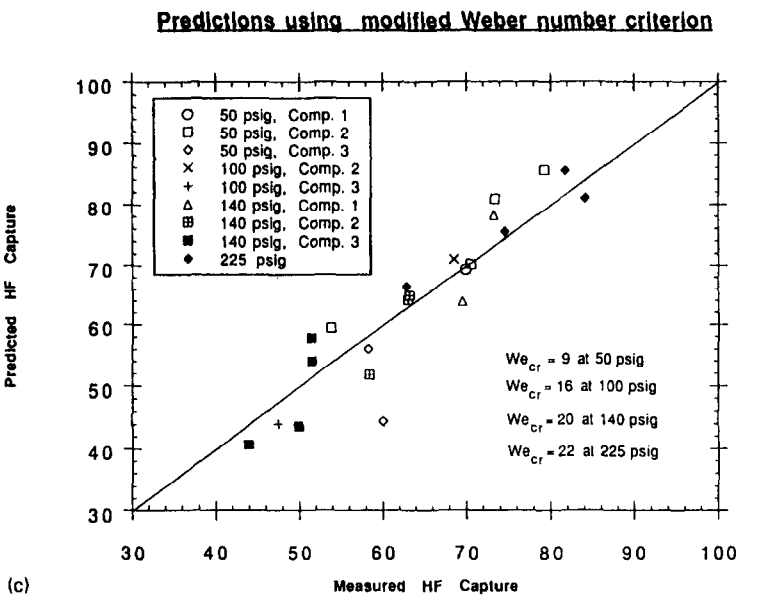

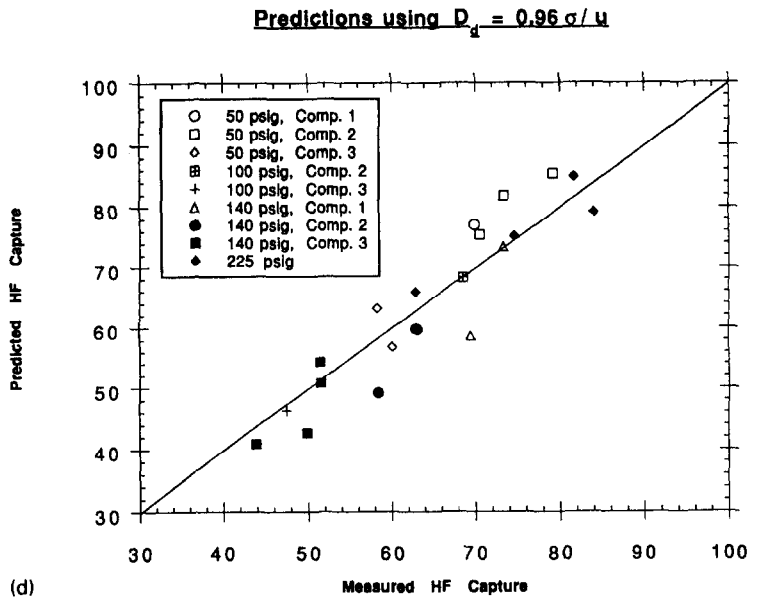

Fig. 6. Continued.

Simple Weber number criterion

Commonly, the characteristic droplet size has been assumed to be given by a Weber number criterion [3–5]. The Weber number (*We*) represents the ratio of the inertial forces causing drop deformation and the restoring capillary forces and is given

by

$$We = \frac{\rho_a u_r^2 D_{d0}}{2\sigma} \sim \frac{\rho_q P D_{d0}}{\rho_l \sigma},$$

where ρ_l and ρ_a are, respectively, the densities of the droplet phase and medium surrounding the droplets, u_r is the speed of the drop relative to the surrounding medium, σ is the surface tension and D_{d0} is the initial drop diameter. The Weber number criterion sets its value at some fixed value (referred to as a critical Weber number). This fixed value is used to determine the drop size. The critical Weber number is expected to be in the range 10–20. Fig. 6(b) shows the predicted rainouts using this criterion compared with the Quest test data. The legend only shows the conditions held constant in the tests and other variables in general were different. By trial and error, a value of 14 for the critical Weber number was found to give a reasonable fit of the data. Although moderate agreement is observed (average absolute deviation of measured from predicted capture is 10), the HF rainouts for 50 psig releases are overpredicted and those for 140 psig are underpredicted. This implies that this criterion over corrects the drop size for pressure. The results of Figs. 6(a) and (b) (no pressure dependence on drop size) imply that the drop size may show a weaker dependence on release velocity.

Modified Weber number criterion

We assume that the critical Weber number is dependent on the release pressure. Fig. 6(c) shows the model predictions compared with the Quest test data. As before, the legend only shows the conditions that were held constant. Critical Weber numbers of 8.5, 16, 20 and 22 have been used for 50, 100, 140 and 225 psig release pressures, respectively. We see that excellent agreement is obtained. The average absolute deviation of predicted capture from experimentally measured value is 4.2. These results indicate that the drop size more closely varies inversely as the release velocity rather than being inversely proportional to the square of the release velocity (simple Weber number criterion).

Drop size proportional to surface tension and inverse of release velocity

The drop size is determined from

$$D_{d0} = \text{constant} \times \frac{\sigma}{u_0}.$$

The predictions are compared in Fig. 6(d) to the data. Again, the legend only shows conditions that were held fixed. Good agreement is observed with average absolute deviation of the predicted values from the measured captures of 4.7.

In summary, a constant drop size for all compositions and release conditions gives agreement with Quest test data for catalyst compositions 2 and 3. The simple Weber number criterion overpredicts the effect of release velocity (pressure). A modified Weber number criterion (with drop size proportional to surface tension and weakly dependent on pressure) gives the best fit of the data and making the drop size

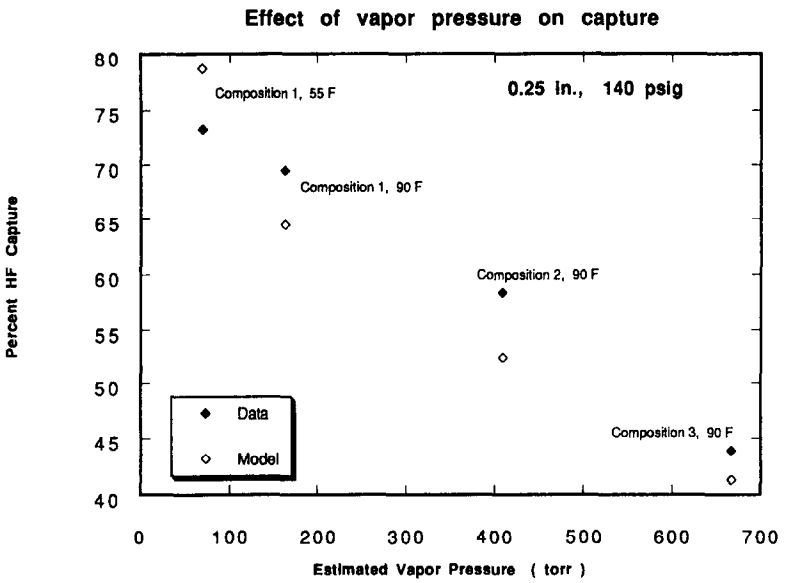

Fig. 7. Effect of vapor pressure on capture.

proportional to the surface tension and inversely proportional to release velocity gives a comparable fit of the data.

3.2. *Interpretation of effect of variables*

The primary variables are the release stream vapor pressure, orifice size, release pressure and release stream temperature. We now interpret the effect of these variables within the framework of the model. In all cases, the modified Weber number criterion is employed.

Vapor pressure

Fig. 7 shows the HF rainout plotted against the release mixture vapor pressure. The data and the model show that the rainout decreases with increasing vapor pressure. This is because, increasing vapor pressure increases the driving force for HF evaporation from the drops.

Orifice size

Fig. 8 shows the HF rainout for different orifice sizes. Both the data and the model show that increasing orifice size increases rainout, although the model appears to show a stronger dependence. The orifice size influences the extent of air entrained-per unit mass of released material (specific air entrainment) and thus influences the driving force for mass transfer. The liquid discharge rate from the orifice, m_l, is

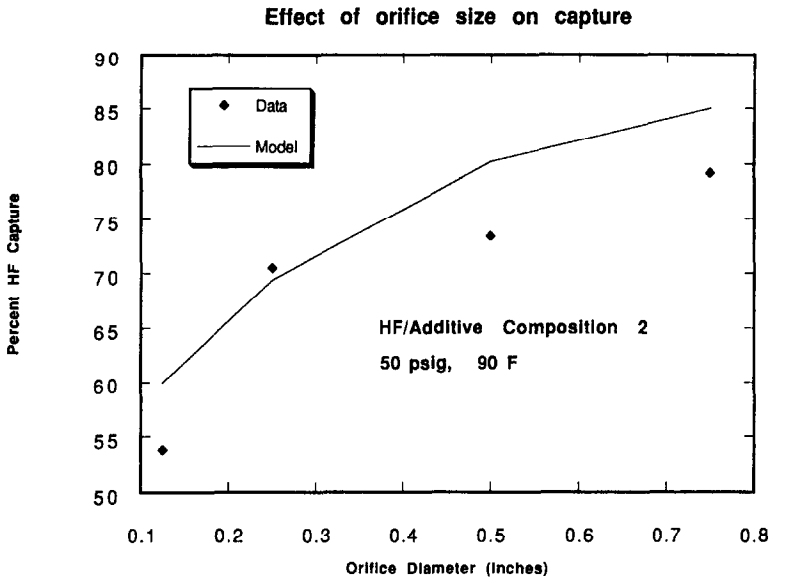

Fig. 8. Effect of orifice size on capture.

given by

$$m_l = \pi d_o^2 \rho_l u_0/4,$$

where d_o is the orifice diameter, ρ_l is the release liquid mass density and u_0 is the liquid release velocity. According to Ricou and Spalding [8], the air entrainment rate per unit distance is given by

$$\frac{dm_a}{ds} = K(\rho_a M)^{0.5},$$

where M is the excess momentum flux and ρ_a is the ambient density and K is a constant. Approximating the ambient density as a constant (strictly the fog density varies with position) and approximating the excess momentum flux with its value at the orifice ($\pi d_o^2 u_0^2 \rho_l/4$), we find that

$$\frac{1}{m_l}\left(\frac{dm_a}{dx} \sim \frac{\rho_a}{\rho_l}\right)^{0.5} \frac{1}{d_o}.$$

Thus the specific air entrainment per unit mass of released liquid increases with decreasing orifice size. This in turn implies a drop surrounding more dilute in HF and as such increased HF evaporation.

Release pressure

According to the above analysis, the air entrainment rate per unit distance per unit mass of released material is independent of the release velocity and hence the release

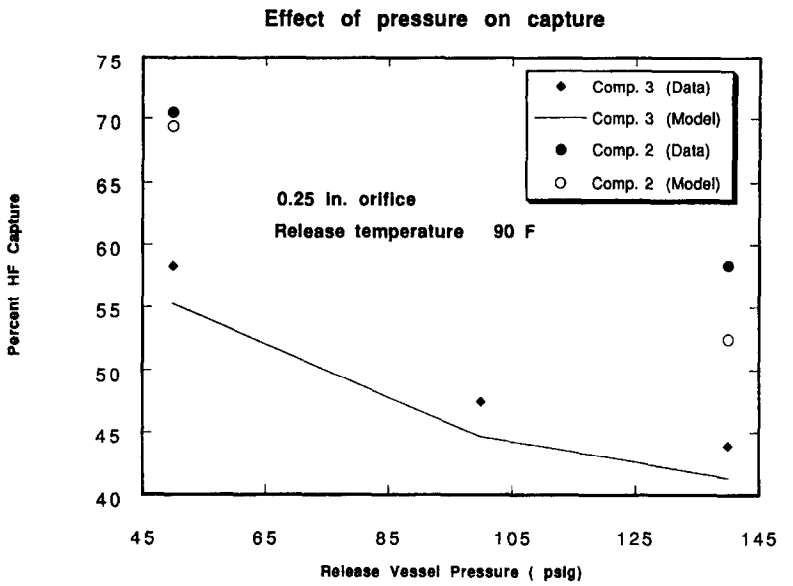

Fig. 9. Effect of pressure on capture.

pressure. Increasing pressure however, causes the jet to travel further and eventually entrain more air. This causes the rainout to be reduced on increasing pressure. Another factor contributing to decreased rainout at higher pressures is the decrease in characteristic drop size. Fig. 9 confirms this dependence of HF rainout on the release pressure.

Release temperature and vapor-phase chemistry

The release stream temperature has a complex influence on HF rainout. This is because of the effect of vapor-phase chemistry. Two sets of tests (Composition 1 at 55 °F and 90 °F and Composition 3 at 78 °F versus Composition 2 at 110 °F) were performed at Quest to assess the effect of release mix temperature on HF rainout.

Fig. 10(a) shows the HF rainouts plotted versus the release mix vapor pressure. For the Composition 1 case, the data and the model show an increase in rainout with decreasing temperature. The model shows a much stronger temperature dependence. Interestingly enough, Composition 3 at 78 °F yields a lower rainout than Composition 2 at 110 °F although it has a slightly lower vapor pressure than the Composition 2 mix at 110 °F. The model also predicts this apparent anomaly.

The higher HF rainout obtained for Composition 2 (110 °F) over Composition 3 (78 °F) can be attributed to the vapor-phase HF oligomerization effects. Although the two mixtures have similar vapor pressures, the effects of HF oligomerization are more pronounced at 78 °F (the oligomerization equilibrium is favored at a lower temperature). This leads to a greater flux of HF (MW = 20.01) for the Composition 3 case than for the Composition 2 case. To verify this hypothesis, the model

calculations were repeated by neglecting vapor-phase chemistry effects. Fig. 10(b) shows the calculations of Figure 10a repeated without the vapor-phase chemistry. The Composition 1 case results remain virtually unchanged because oligomerization effects are small at these vapor pressures. The trends for the Composition 3 (78 °F) and

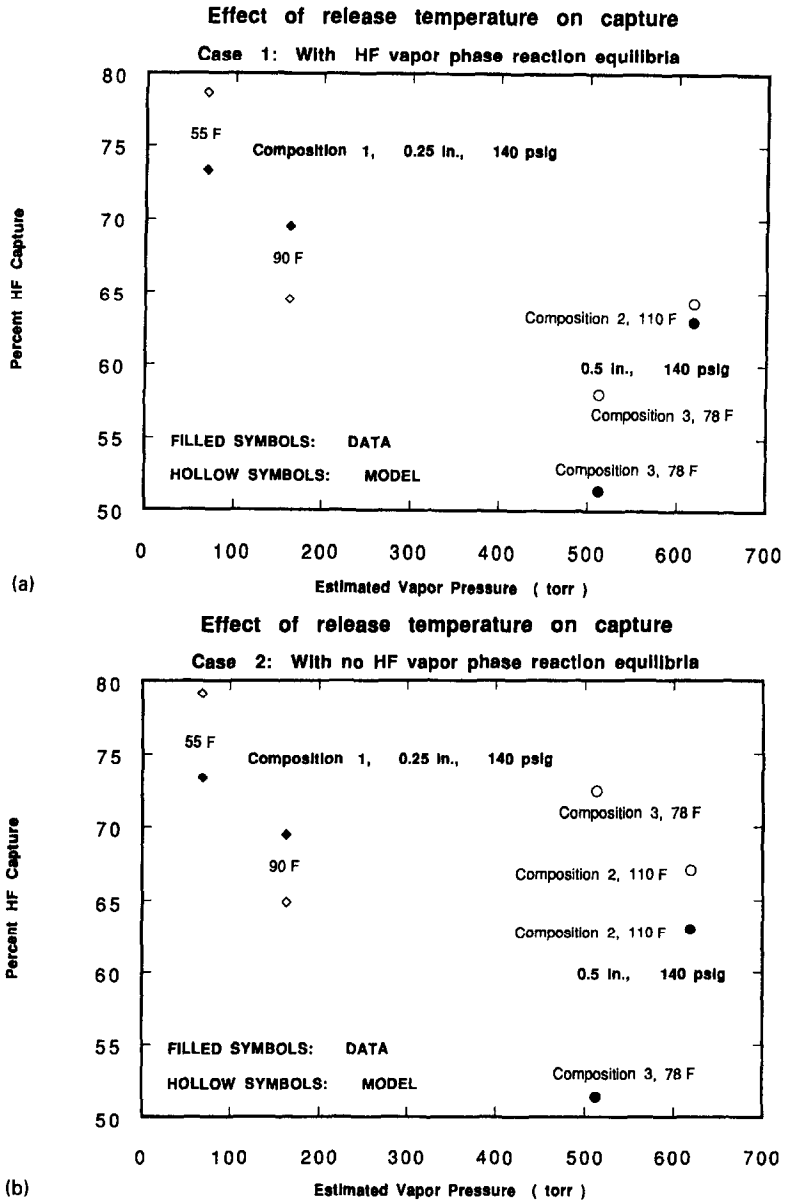

Fig. 10. (a) Effect of release temperature on capture. Case 1: With HF vapor phase reaction equilibria. (b) Effect of release temperature on capture. Case 2: With no HF vapor phase reaction equilibria.

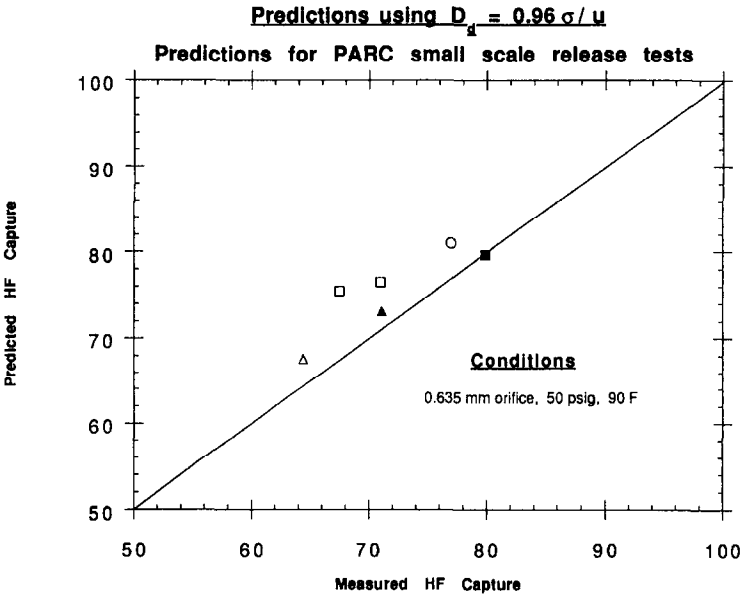

Fig. 11. Predictions using $D_d = 0.96\sigma/u$. Predictions for PARC small scale release tests.

Composition 2 (110 °F) are reversed with respect to Fig. 10(a). Thus, in the absence of vapor-phase chemistry, Composition 3 at 78 °F yields a higher rainout than Composition 2 at 110 °F because of its lower vapor pressure. This exemplifies the need to accurately describe the vapor-phase chemistry for HF in the release model.

3.3. Model evaluation using laboratory release data

Small scale HF/additive release experiments were performed in a flow chamber at Pittsburgh Applied Research Corporation (PARC). The orifice diameter was 0.635 mm (1/40 in) and the release pressure was approximately 50 psig. The flow chamber was approximately 1 m long. The rainout liquid was collected in pans filled with water.

Fig. 11 shows the HF captures compared to experimental values. The different points correspond to different tested compositions. Since the mass release rate was measured, the drop size was estimated using the same correlation as that used to generate Fig. 6(d) (drop size = 0.96 σ/u). Good agreement is observed.

4. Other model predictions

The model can be used to study the fog properties, effect of ambient variables and as an aid for release flow chamber design.

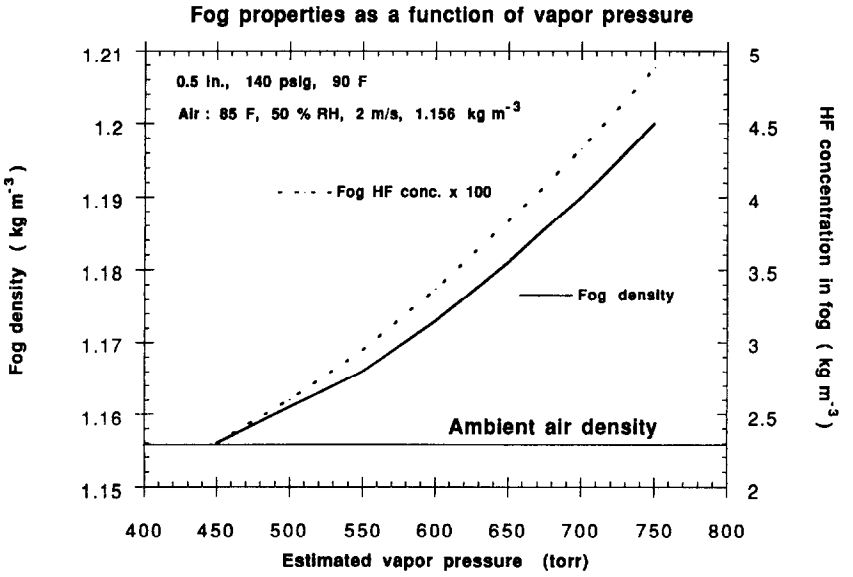

Fig. 12. Fog properties as a function of vapor pressure.

4.1. *Fog properties*

The fog flow rate and momentum as well as the fog properties (temperature, density and composition) are part of the solution obtained from the model. These properties may be used to initialize atmospheric fog dispersion calculations for risk assessment applications in situations where there is appreciable liquid rainout. For example, this release model can become a front end of a more general model that continues the atmospheric fog dispersion calculations after the liquid has rained out on the ground.

Fig. 12 depicts the fog density (at the location of rainout) as a function of the release stream vapor pressure for releases at 140 psig and 90 °F through a half-inch orifice. On the same graph, the corresponding HF concentrations in the fog are also shown. As expected, fog density as well as HF fog concentration increase with increasing vapor pressure. This is due to two reasons. The increasing vapor pressure promotes HF evaporation from the drops and contributes to increasing aerosol formation. Further, increasing vapor pressure by increasing HF concentration in the release stream, decreases the air-to-HF weight ratio in the fog. This also contributes to an increase in fog density.

4.2. *Influence of ambient air conditions*

The ambient air temperature and humidity influence the fog properties and this influences the heat and mass transfer rates and as such the HF rainout. The wind velocity influences the air entrainment into the jet and thereby affects HF rainout.

Fig. 13(a) shows the dependence of HF capture on ambient air temperature at fixed relative humidity. The results correspond to a HF/additive Composition 2 release at 140 psig and 90 °F through a 0.5 in orifice. We see an increase in HF rainout with decreasing air temperature. This is because decreasing air temperature results in decreased heat transferred to the drops and as such colder drops. Further, increasing air temperature at fixed relative humidity increases the total moisture in air and this leads to increased aerosol formation and increased HF evaporation from drops.

The dependence of ambient relative humidity on HF rainout is studied in Fig. 13(b). As the humidity increases, HF rainout decreases. This is because increasing humidity promotes aerosol formation. This condensation increases the fog temperature and this in turn heats the drop. Further, the fog vapor becomes depleted of HF as the HF goes into the aerosol. This increases the driving force for HF evaporation from the drops. This trend of decreasing HF capture with increasing humidity was observed in the large-scale Quest HF/additive tests. The first phase of these tests were conducted with recirculating air in a closed chamber. The air was constantly humidified with the water sprays. This essentially water vapor saturated environment yielded lower rainouts than the tests conducted with ambient air flowing through the chamber.

The effect of air speed is illustrated in Fig. 13(c). The HF capture is essentially not impacted by typical variations in air speed. The HF evaporation is influenced by the specific air entrainment (entrainment rate per unit distance), overall air entrained and residence time. With increasing air speed, although the specific entrainment rate is reduced, the jet traverses farther (because the reduced entrainment slows the jet less) and the overall entrainment is probably not significantly impacted.

4.3. Effect of restricted air entrainment

As discussed in Section 2, a turbulent free jet entrains air from the surrounding and expands. This section studies the consequence of limiting the available air for entrainment at some fixed value. This study has significance in the correct design and interpretation of flow chamber release experiments. In a flow chamber of fixed geometry, the available air for entrainment depends on the chamber cross-sectional area and the air speed through the chamber. For larger orifice releases and at higher pressures, air entrainment could become restricted. To study this effect, we fixed the air flow through the chamber at different values and calculated the rainout using the model. The entrainment is assumed to occur unhindered until the quantity entrained equals the air flow. At this point the entrainment is shut off. However, the jet and droplet balances are continued to be solved till the jet centerline strikes the ground.

Fig. 14 shows the HF rainout versus airflow for the case of a Composition 3 release through a half-inch orifice at 140 psig. As expected, the rainout increases as the available air for entrainment is decreased. This is due to two reasons. First, a lower air to release liquid weight ratio results in a fog vapor more saturated in HF and this

lowers the rate of HF evaporation from the drops. Second, it also results in a higher two-phase jet density and this causes the jet to settle more rapidly thus reducing the residence time. The effect is more severe for small air flows because the driving force for HF evaporation is substantially reduced.

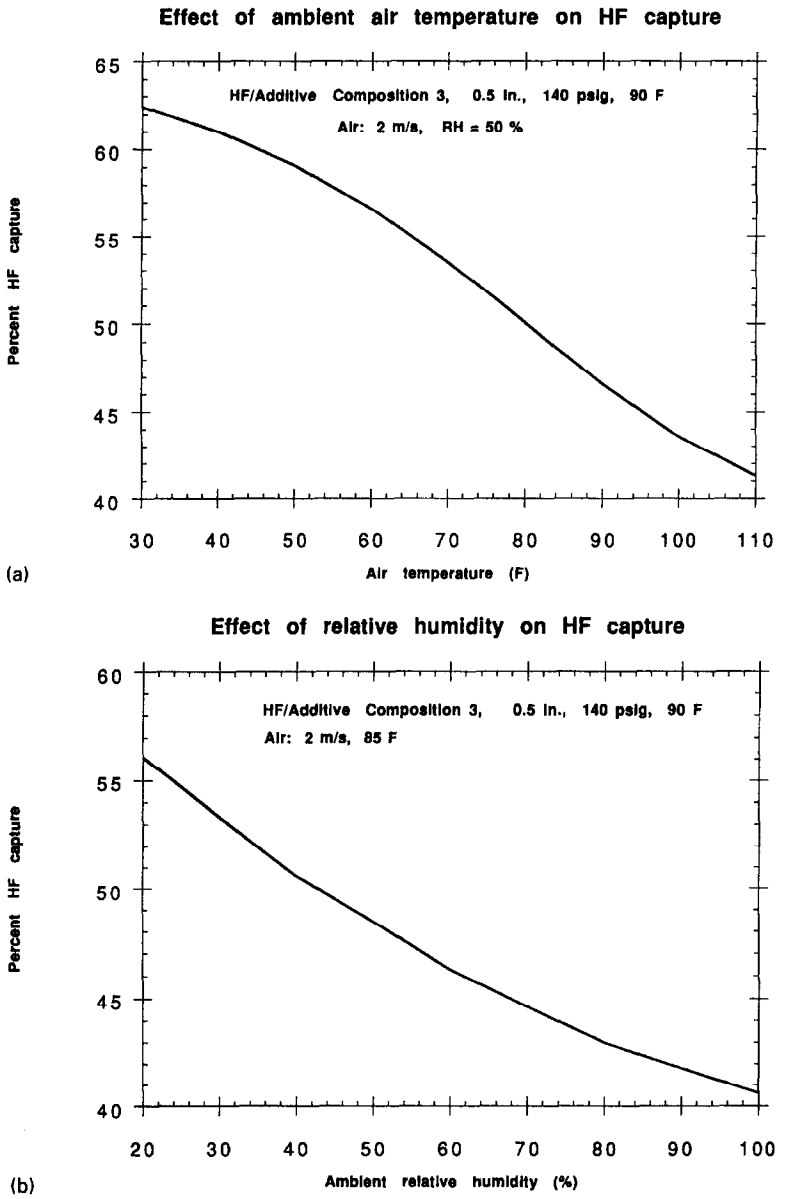

Fig. 13. (a) Effect of ambient air temperature on HF capture. (b) Effect of relative humidity on HF capture. (c) Effect of air speed on HF capture.

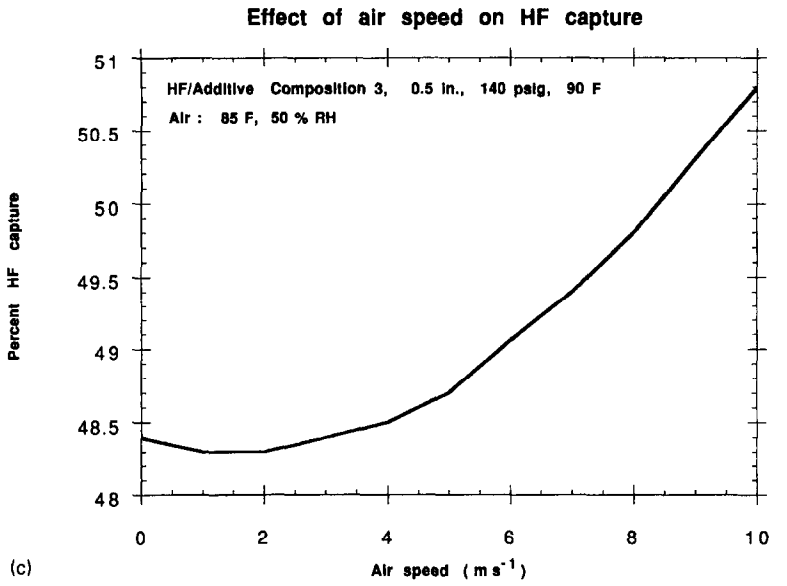

Fig. 13. Continued.

5. Equilibrium with two liquid phases

We have investigated the complete equilibration of an HF/additive jet with a fixed quantity of entrained air [14] as a generalization of the well known Schotte Model [6]. The model solution in general consisted of one liquid phase and one vapor phase. Aerosol release tests have shown two liquid phases to be present. The first liquid phase consisting of large droplets rains out on the ground. The second liquid phase is airborne as a vapor–liquid fog and its presence renders the fog visible. The limitation of restricting to one liquid phase in the Schotte model (complete equilibration) implies that one cannot simultaneously describe both the phenomenon of rainout and that of vapor–liquid fog formation. Thus, if the liquid phase is assumed to be present as large drops, they rainout and there is no aerosol. On the other hand, if the drops are assumed to be small enough to be airborne, then there is no rainout and there is only a vapor–liquid aerosol.

An equilibrium solution with two liquid phases yielding an upper bound on the aerosol formation may be obtained from this model by the application of a suitable constraint. To obtain this solution, artificial constraints in the form of no water exchange between the phases (mass transfer coefficient for water is zero) and no interaction between the fog liquid phase and the parent drop phase are introduced. HF evaporating from the drops interacts with moisture in the humid air to form the aerosol (liquid + vapor). The aerosol particles are assumed not to interact with the parent drops and thus any exchange between the aerosol particles and parent drops is neglected. Thus complete equilibration is prevented. (On a sufficiently long timescale

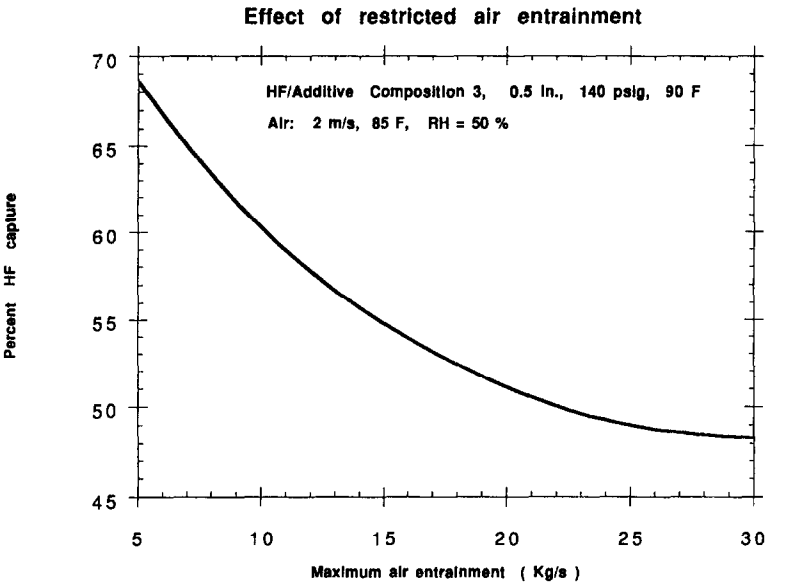

Fig. 14. Effect of restricted air entrainment.

Brownian diffusion of aerosol particles and collisions between parent drops and aerosol particles will lead to an equilibrium with a single liquid phase.) The absence of water condensation into the drops makes all the water vapor in humid air available for aerosol formation and thus the conditions are most favorable for aerosol formation. After the jet has accumulated the specified amount of air (determined by solving the two-phase jet model until the jet strikes the ground), entrainment and gravity are shut off but the transport equations are solved until the closed system (released material + entrained air) approaches equilibrium. This is indicated by the thermal equilibration between the parent drop phase and the fog phase.

Fig. 15 shows the fraction of initial HF in drops, drop and fog temperatures as a function of distance from the orifice for a Composition 3 release. The results suggest a thermal equilibration of the fog phase and the parent liquid drop phase. The asymptotic HF capture (defined as the HF in parent drop phase) appears to be around 20%. The experimental value was 51.5%. It thus appears that the two-liquid phase equilibrium model yields an upper bound on airborne HF or aerosol formation.

6. Summary and conclusions

This paper describes a two-phase jet model that may be used to understand the behavior of HF/additive releases and provide input to risk assessment and fog dispersion models. This model is a generalization of that of Papadourakis et al. [4]

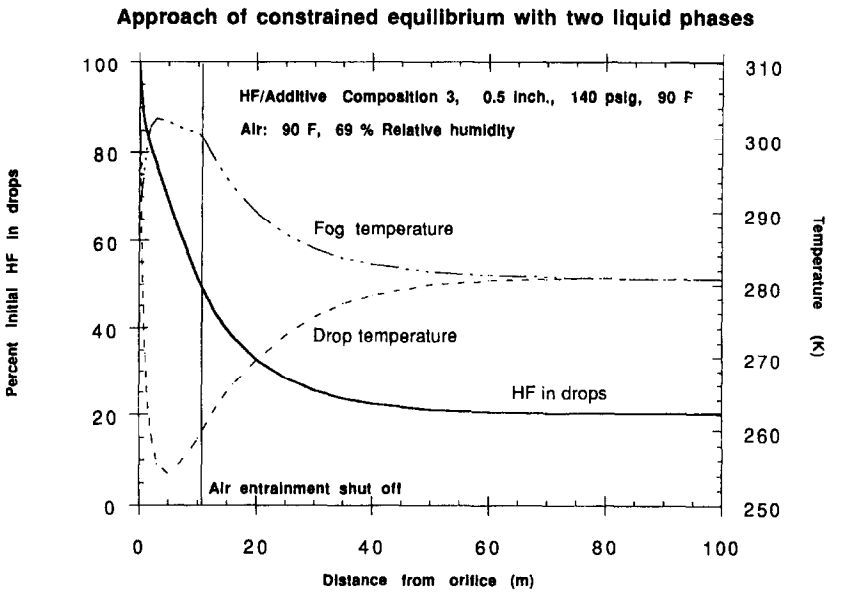

Fig. 15. Approach of constrained equilibrium with two liquid phases.

and Woodward and Papadourakis [5]. The key conceptual element unique to this work is the accurate description of the fog phase (accounting for HF vapor-phase oligomerization and HF–water complex formation equilibria along with liquid-phase formation). Such an accurate description is necessary to accurately predict the transport processes between the parent drops and the surrounding fog. Moreover, the knowledge of the fog properties are necessary to initialize atmospheric fog dispersion models. This work also presents the first substantial effort at modeling multicomponent releases that has been substantiated with extensive experimental data. Of particular importance is the dependence of fractional HF retained in the drops as a function of distance from the orifice. Another salient aspect of this work is the generalization of the equilibrium Schotte model [6, 14] to a system forming two liquid phases. The solution of this model comes by marching the jet model solution to equilibrium. This equilibrium solution yields a lower bound on the HF rainout or the upper bound on the aerosol formation.

The initial parent drop size is an input to the model and different strategies for estimating this are evaluated. While the simple Weber number criterion provides a reasonable prediction of the data, it appears to overestimate the dependence on drop size with release velocity. Much better agreement is observed for large and small scale releases by making the drop size proportional to the surface tension and inversely proportional to the release velocity. The studies emphasize that an adequate description of transport phenomena, fog equilibria, HF vapor-phase chemistry, jet trajectory and drop size dependence on physical properties and release conditions are necessary to describe experimental observations.

There are areas for further improvement of the model. These include (i) drop size correlation derived from detailed measurements of drop size distributions near the orifice, (ii) accounting for any relative motion between the drops and the fog which could be important for low pressure releases and (iii) tighter VLE model parameters obtained from data over a wider range of compositions and temperature. These improvements will be addressed in future publications as more data become available. The model is also being generalized to handle flashing jets. Such jets may disintegrate by flash atomization producing very small droplets [15]. While the physics of drop evaporation presented in this paper apply for such releases as well, the drop size correlations discussed here may not be appropriate. While the applications in this paper are on subcooled jets, it has been found that the model also describes superheated HF/additive releases that do not flash atomize. Such applications will be addressed in future publications.

Appendix A: HF/additive/water thermodynamics and fog equilibrium

A.1. HF/additive/water thermodynamics

Determination of the vapor compositions at a liquid–vapor interface and also the fog properties requires an adequate representation of the HF/additive/water system thermodynamics. The following assumptions are made [14]:

1. The HF/additive/water liquid phase nonidealities may be described by the Non-Random Two Liquid (NRTL) liquid activity coefficient model [16]. In a 5-parameter version of this model, the liquid-phase excess molar free energy of an n-component system is given by

$$\frac{\tilde{G}^{E}}{RT} = \sum_{i=1}^{k=n} x_i \frac{\sum_{k=1}^{k=n} \tau_{ki} G_{ki} x_k}{\sum_{k=1}^{k=n} G_{ki} x_k}.$$

In the above, R is the universal gas constant, T is the absolute temperature, x_j $j = 1, \ldots, n$ are the liquid phase mole fractions and

$$\tau_{ij} = a_{ij} + b_{ij}/T, \quad G_{ij} = e^{-\alpha_{ij}\tau_{ij}}, \quad i, j = 1, \ldots n,$$

where a_{ij}, b_{ij} and α_{ij} are binary parameters that may be regressed from binary VLE data. In a 3-parameter version, the parameters, a_{ij} and a_{ji}, are set equal to zero. The liquid-phase activity coefficients and heats of mixing (excess enthalpy) follow readily from the thermodynamic identities

$$\ln \gamma_i = \frac{\partial}{\partial n_i}\left(\frac{n\tilde{G}^{E}}{RT}\right)_{T,p,n_j \neq n_i}, \quad \frac{\tilde{H}^{E}}{RT} = -T\frac{\partial}{\partial T}\left(\frac{\tilde{G}^{E}}{RT}\right)_{p,x_j \quad j=1,\ldots,n},$$

where n_j, $j = 1, \ldots, n$ are mole numbers and n is the total number of moles. Often separate sets of binary parameters are required for predicting vapor pressures and heats of mixing, especially if reaction equilibria in the vapor phase mask the true liquid-phase activity coefficients. The parameters used in these calculations are the

same as those given in Ref. [14].

2. The increase in vapor pressure of HF in droplets relative to bulk liquid of the same composition is neglected. The errors from this approximation are expected to be less than 0.1% [6].

3. An accurate description of the enthalpic effects associated with fog formation requires a detailed treatment of the HF vapor-phase chemistry [6]. HF in the vapor phase is assumed to exist as an equilibrium mixture of monomer, dimer, hexamer, octamer and $HF \cdot H_2O$ complex [6].

4. Other than HF oligomerization effects and HF–water complex formation, the vapor phase is assumed to behave ideally. In other words, the fugacity coefficient of each of the species in the vapor phase is assumed to be unity. In view of the fact that the pressure during this mixing (atmospheric) is small, any errors from this assumption are expected to be small.

5. The excess volume of mixing and excess heat capacities of the liquid phase are neglected. The Poynting factor is set to unity and temperature dependencies of the heat capacities are neglected.

The assumptions on the liquid and vapor phase behavior imply that the vapor–liquid equilibrium is described by

$$Py_i = x_i \gamma_i P_i^{\text{sat}}, \quad i = \text{HF, additive, } H_2O, \tag{A.1}$$

where $\{y_i\}$, $\{x_i\}$ and $\{P_i^{\text{sat}}\}$ are, respectively, the vapor-phase mole fractions, the liquid phase mole fractions and the pure component saturation pressures. Since HF in the vapor phase exists as an equilibrium mixture of oligomers and HF–water complex, the partial pressures of HF (P_{HF}) and water (P_{w}) need to be defined. These partial pressures are related to the oligomer partial pressures $\{P_{(\text{HF})}\}_{i=1,2,6,8}$, HF–water complex partial pressure (P_{c}) and pure water partial pressure ($P_{\text{w,pure}}$) as

$$P_{\text{HF}} = P_{(\text{HF})_1} + P_{(\text{HF})_2} + P_{(\text{HF})_6} + P_{(\text{HF})_8} + \beta_1 P_{\text{c}}, \tag{A.2a}$$

$$P_{\text{w}} = P_{\text{w,pure}} + \beta_2 P_{\text{c}}, \tag{A.2b}$$

where β_1 and β_2 are assumed to be related to the molecular weights of HF and water (MW_{HF} and MW_{w}) by

$$\beta_1 = \text{MW}_{\text{HF}}/(\text{MW}_{\text{HF}} + \text{MW}_{\text{w}}), \qquad \beta_2 = \text{MW}_{\text{w}}/(\text{MW}_{\text{HF}} + \text{MW}_{\text{w}}).$$

The reference temperature is 25 °C and the reference state for HF is ideal monomer vapor. For other components, the reference state is that of an ideal gas.

A.2. Fog equilibrium calculations

The fog properties at any axial position, s, are determined from an assumption of local equilibrium. The equilibration of a mixture of HF, additive, water and dry air of specified enthalpy and fixed total pressure results in general in a vapor–liquid fog. The fog properties to be determined are its temperature (tc or T_{f}), liquid or aerosol droplet volume fraction (f_{l}), liquid compositions (x_i, $i = 1, 2, 3$), vapor compositions (y_i, $i = 1, 2, 3, 4$) and volumetric flow rate of fog (v_{f}).

The molar feed rates of the four species (ζ_i in the fog, $i = 1, \ldots, 4$) and the total enthalpy (ψ in the fog) are known at any axial location, s, from material and energy balances (see Section 2.3). These flows along with the requirement of reversible adiabatic and isobaric mixing, completely specify the problem of determining the fog properties and flow rates. The final conditions are determined from the requirement that the total system pressure be atmospheric and

$$H_{\text{final}} = \psi. \tag{A.3}$$

In order to solve this problem, it is necessary to express the enthalpy at any temperature. The total enthalpy (H_{final}) of the mixed system at any temperature, t_c (Celsius), is given by

$$H_{\text{final}} = H_{\text{vap}} + H_{\text{liq}}. \tag{A.4}$$

The vapor enthalpy (H_{vap}) can be expressed as

$$H_{\text{vap}} = M_a h_a + \frac{(h_{\text{HF}} Y_{\text{HF}} + h_{\text{add}} Y_{\text{add}} + h_w Y_w)}{Y_{\text{HF}} + Y_{\text{add}} + Y_w} \phi_v (M_{\text{HF}} + M_{\text{add}} + M_w)$$

with the total molar flows and vapor and liquid molar rates given by

$$\zeta_{\text{HF}} = M^v_{\text{HF}} + M^l_{\text{HF}},$$

$$\zeta_{\text{add}} = M^v_{\text{add}} + M^l_{\text{add}},$$

$$\zeta_w = M^v_w + M^l_w$$

and the fog vapor molar enthalpies (MW HF = 20.01) given by

$$h_a = \text{Cp}^g_a (t_c - 25), \qquad \text{Cp}^g_a = 6.96 \text{ cal/(gmol K)},$$

$$h_w = \text{Cp}^g_w (t_c - 25), \qquad \text{Cp}^g_w = 8.05 \text{ cal/(gmol K)},$$

$$h_{\text{add}} = \text{Cp}^g_{\text{add}} (t_c - 25),$$

$$h_{\text{HF}} = \text{Cp}^g_{\text{HF}} (t_c - 25) + \Delta, \qquad \text{Cp}^g_{\text{HF}} = 6.96 \text{ cal/(gmol K)}.$$

In the expression for the total vapor enthalpy, ϕ_v is the fraction of total moles of HF, additive and water that is vaporized and Δ is the enthalpy deviation function for HF from ideal monomeric state (MW = 20.01) at temperature "t_c". This enthalpy deviation is given by

$$\Delta = \frac{y_{12}\Delta H_2 + y_{16}\Delta H_6 + y_{18}\Delta H_8 + y_c \Delta H_c}{y_{11} + 2y_{12} + 6y_{16} + 8y_{18} + y_c} \tag{A.5}$$

where $\{y_{1i}\}$, $i = 1, 2, 6, 8$ are the HF oligomer vapor mole fractions and y_c is the HF–water complex mole fraction.

The fog liquid enthalpy is given by

$$H_{\text{liq}} = (1 - \phi_v)(\zeta_{\text{HF}} + \zeta_{\text{add}} + \zeta_w) H_l$$

where the liquid-phase molar enthalpy is given by

$$H_l = Cp^l(t_c - 25) - \Delta_{25}.$$

Denoting the heats of vaporization of HF, additive and water by Q_{HF}, Q_{add} and Q_w respectively and letting H^E denote the molar excess enthalpy of the liquid, we have

$$\Delta_{25} = x_{HF}Q_{HF} + x_{ad}Q_{ad} + x_wQ_w - H^E \tag{A.6}$$

$$Q_{HF} = 7231 \text{ cal/gmol}, \qquad Q_w = 10519 \text{ cal/gmol}.$$

The liquid molar average specific heat (Cp^l) given by

$$Cp^l = x_{HF}Cp^l_{HF} + x_{ad}Cp^l_{ad} + x_wCp^l_w. \tag{A.7}$$

Estimation of the enthalpy deviation function, Δ, requires the knowledge of HF oligomerization and HF–water complexation equilibria. These reactions are described by Ref. [6]

$$2HF \Leftrightarrow HF_2, \qquad K_2 = \exp\left(\frac{12775.229}{RT} - \frac{47.97731}{R}\right), \tag{A.8a}$$

$$6HF \Leftrightarrow HF_6, \qquad K_6 = \exp\left(\frac{41927.495}{RT} - \frac{138.5519}{R}\right), \tag{A.8b}$$

$$8HF \Leftrightarrow HF_8, \qquad K_8 = \exp\left(\frac{50120.984}{RT} - \frac{165.8526}{R}\right), \tag{A.8c}$$

$$HF + H_2O \Leftrightarrow HF \cdot H_2O, \qquad K_c = \exp\left(\frac{6266}{RT} - \frac{22700}{R}\right), \tag{A.8d}$$

where the ΔH values are the the negative of the first constants appearing in the expressions for the equilibrium constants. The calculation of the enthalpy deviation therefore requires the knowledge of the individual species mole fractions. Since

$$P_l = P_{HF} = P_{11} + P_{12} + P_{16} + P_{18} + \beta_1 P_c \tag{A.9}$$

and the oligomer and complex partial pressures are related to that of the monomer via the equilibrium constants, we have on letting $f_1 = P_{11}$

$$\Phi(f_1) = f_1 + K_2 f_1^2 + K_6 f_1^6 + K_8 f_1^8 + \beta_1 \frac{K_c f_1 P_w}{1 + \beta_2 K_c f_1} - P_{HF} = 0. \tag{A.10}$$

The above may be solved for the monomer partial pressure by Newton–Raphson iteration once the equilibrium HF partial pressure P_l and the temperature are known. The individual mole fractions are then readily obtained from the knowledge of the equilibrium constants.

A.3. Solution procedure

The solution of the above set of equations consists of the final temperature, fog liquid and vapor fractions and the individual phase compositions. It consists of a sequence of nested Newton–Raphson iterations. The outer loop solves the enthalpy

balance and converges on the final temperature (HP flash). The nested inner loop solves material balance and VLE equations that converges on the liquid fraction and the two-phase compositions (TP flash). The solution procedure is started by estimating the final temperature. Using this temperature and ambient pressure, one performs the TP flash by solving the following material balances:

$$z_j = \beta Y_j + (1 - \beta)x_j, \quad j = 1,2,3,4,$$

where $\{z_j\}$ are the overall mole fractions in the fog (based on HF molecular weight of 20.01). The apparent vapor mole fractions and liquid-phase mole fractions satisfy

$$\sum_{i=1}^{n} Y_i = \sum_{i=1}^{n} x_i = 1.$$

In addition, VLE relations for the are expressed by

$$K_i^{\text{app}} = Y_i/x_i, \quad i = 1,2,3,4.$$

These apparent K values for the HF, additive and water are given by

$$K_i^{\text{app}} = P_{i,\text{app}}^{\text{sat}}/x_i P_{\text{app}}, \quad i = 1,2,3.$$

The real K value of air is taken as

$$K_a = 50\,000/P.$$

The K values are initialized using Raoult's law. Once the TP flash has converged, the liquid and vapor fractions as well as the compositions are known. The actual monomer vapor-phase composition may be found using Eq. (A.9) and the oligomer and complex fractions via the equilibrium relationships (A.8a)–(A.8d). The total fog enthalpy is then determined via (A.4). If condition (A.3) is not satisfied, a new temperature is determined by a Newton–Raphson scheme.

A.4. Fog property calculation

Once the equilibrium solution has been determined, the fog vapor and liquid densities (ρ_{fv} and ρ_{fl}) as well as the overall fog density (ρ_{f}) may be readily calculated. Let F denote the total molar flow rate (HF + additive + water + dry air) and let z_{HF}, z_{add}, z_{w} and z_{a} denote the overall mole fractions (HF molecular weight = 20.01). Let ϕ_{l} denote the fraction of the moles of HF, additive and water that is liquid. Denoting the liquid molar flow rate by L,

$$\phi_1 = \frac{L(x_{\text{HF}} + x_{\text{add}} + x_{\text{w}})}{F(z_{\text{HF}} + z_{\text{add}} + z_{\text{w}})} = 1 - \phi_{\text{v}}.$$

Defining the fraction of the total moles (HF + additive + water + dry air) that is vaporized by v, we have

$$1 - v = L/F.$$

Using the above,

$$\phi_1 = (1 - v)\frac{(x_{HF} + x_{add} + x_w)}{(z_{HF} + z_{add} + z_w)}.$$

The fog liquid mass density, ρ_{fl}, is given by

$$\rho_{fl} = \frac{20.01x_{HF} + 18.02x_w + MW_{add}x_{add} + 28.97x_a}{x_{HF}V_{HF} + x_wV_w + x_{add}V_{add} + x_aV_a},$$

where V_{HF}, V_{add}, V_w and V_a are, respectively, the liquid molar volumes of HF, additive, water and air. The liquid mass flow, w_l, is computed as

$$w_l = (1 - v)F\,MW_l$$

where MW_l is the average liquid molecular weight given by

$$MW_l = 20.01x_{HF} + 18.02x_w + x_{add}\,MW_{add} + 28.97x_a.$$

Thus the volumetric flow rate of fog liquid, v_{fl}, may be computed as

$$v_{fl} = \frac{w_l}{\rho_{fl}} = \frac{(1 - v)F\,MW_l}{\rho_{fl}}.$$

The fog vapor mass flow rate, w_v, is given by

$$w_v = F\,MW_F - w_l,$$

where MW_F is the feed average molecular weight computed as

$$MW_F = 20.01z_{HF} + 18.02z_w + MW_{add}\,z_{add} + 28.97z_a.$$

The fog vapor mass density, ρ_{fv}, is given by

$$\rho_{fv} = \frac{P\,MW_v}{RT},$$

where the vapor average molecular weight, MW_v, is given by

$$MW_v = 20.01(y_{11} + 2y_{12} + 6y_{16} + 8y_{18}) + 18.02y_w + 38.03y_c + MW_{add}\,y_{add} + 28.97y_a.$$

The volumetric flow of fog vapor, v_{fv}, is then obtained as

$$v_{fv} = w_v/\rho_{fv}.$$

The fog liquid volume fraction, f_l, written as

$$f_l = \frac{v_{fl}}{v_{fl} + v_{fv}}.$$

Appendix B: Physical property estimation method

The calculations draw on several pure component and mixture properties. The following is a summary of the estimation methods.

B.1. Vapor pressures

Pure component vapor pressures have been obtained from correlations in NSRDS/AIChE Tables [17]. Liquid solution vapor pressures are predicted using the NRTL liquid activity coefficient model. The NRTL model and parameters are discussed in Ref. [14].

B.2. Ideal gas heat capacities

Constant values corresponding to 25 °C have been obtained from NSRDS/AIChE Tables [17].

B.3. Liquid heat capacities

Pure component values are obtained from correlation in NSRDS/AIChE Tables [17]. The liquid mixture heat capacity is obtained from

$$\mathrm{Cp}_{\mathrm{mix}} = \sum_i x_i \, \mathrm{Cp}_i,$$

where x_i and Cp_i are, respectively, the mole fraction and molar heat capacity of species i. Thus excess heat capacities are set equal to zero.

B.4. Surface tension

The surface tension of pure components is obtained using NSRDS/AIChE Tables [17]. The surface tension of the mixture is given by

$$\sigma_{\mathrm{mix}}^{-1} = \sum_i x_i \sigma_i^{-1},$$

where σ_i is the surface tension of component i in the solution.

B.5. Liquid molar volume

The pure component molar volumes are obtained from NSRDS/AIChE Tables [17]. The solution molar volume is given by

$$V_{\mathrm{mix}} = \sum_i x_i V_i$$

where V_i is the liquid molar volume of species i. Thus any volume change of mixing is neglected.

Nomenclature

Upper case

Cp^g	gas molar heat capacity
Cp^l	liquid molar heat capacity
D	binary diffusivity
D_d	droplet diameter
D_{do}	initial droplet diameter
$\tilde{G}^E$	molar excess Gibbs free energy
$\tilde{H}^E$	molar excess enthalpy
H^a	apparent vapor molar enthalpy
H_{final}	total enthalpy of fog phase
H_{liq}	total enthalpy of fog liquid
H_{vap}	total enthalpy of fog vapor
N_d	number flow rate of drops
P	pressure
Q	normalizing factor showing significance of vapor-phase association of HF
Q_i	heat of vaporization of species i
R	universal gas constant
R_{TP}	two-phase jet radius
T_d	droplet temperature
T_f	fog temperature
T_v	temperature of phase surrounding droplet
U	drop centerline velocity
U_{dx}	drop x velocity
U_{dy}	drop y velocity
U_{TP}	two-phase jet velocity
U_{TPX}	two-phase jet x velocity
Y_{TPY}	two-phase jet y velocity
$X_j(0-)$	X coordinate of orifice
$Y_j(0-)$	Y coordinate of orifice
X_{TP}	two-phase jet centerline x coordinate
Y_{TP}	two-phase jet centerline y coordinate
Y_i	apparent vapor mole fraction of species i as defined in Section 2.1
Y_i^*	apparent vapor mole fraction of species i at the vapor–drop interface

Lower case

d_o	orifice diameter
h_t	heat transfer coefficient
h	molar enthalpy of the vapor phase
h_i	vapor molar enthalpy of species i (HF based on MW = 20.01)
h_d	molar enthalpy of droplet phase
g	acceleration due to gravity

f_v, f_l	fog vapor and fog liquid volume fractions
m_a	air entrainment rate
m_d	total moles present in a droplet
p_x, p_y	two phase jet momenta components
s	centerline coordinate
u_0	release velocity
v_f	fog volumetric flow rate
v_{fv}	fog vapor volumetric flow
v_{fl}	fog liquid volumetric flow
w	wind velocity
w_v, w_l	fog vapor and liquid mass flow rates
x_i	fog liquid mole fraction of species i
y_i	real mole fraction of species i in fog vapor
y_a^0	mole fraction of dry air in ambient air
y_w^0	mole fraction of water vapor in ambient air
z_i	overall mole fraction of species i in fog (HF MW = 20.01)

Greek letters

Δ	enthalpy deviation function
ε	turbulence energy dissipation per unit mass
ε_p	jet droplet volume fraction
ε_{p0}	initial jet droplet volume fraction
ζ_i	molar flow rate of species i in fog (HF MW = 20.01)
θ	angle of jet with respect to horizontal (see Fig. 1)
μ_a	dynamic viscosity of air
ρ_a, ρ_d	air, drop densities
ρ_{TP}	two-phase jet density
ρ_{fv}	density of fog vapor
ρ_{fl}	density of fog liquid
ψ	total fog-phase enthalpy flow
ω_i	parent drop mole fraction of species i
σ	surface tension

References

[1] J.H. Gray and G.E. Handwerk, Petroleum Refining: Technologies and Economics, Marcel Dekker, New York, 2nd edn., 1984.
[2] D.N. Blewitt, J.F. Yohn, R.P. Koopman and T.C. Brown, Paper presented at The Int. Conf. on Vapor Cloud Modeling, Cambridge, MA, 2–4 November 1987.
[3] G.A. Melhem and R. Saini, Paper presented at The AICHE Process Plant Safety Symp., Houston, TX, February, 1992.
[4] A. Papadourakis, H.S. Caram and C.L. Barner, J. Loss Prev. Process Ind., 4 (1991) 93.

[5] J.L. Woodward and A. Papadourakis, in: Int. Conf. and Workshop on Modeling and Mitigating the Consequence of Accidental Releases of Hazardous Materials, New Orleans, LA, 20–24 May 1991, p. 147.
[6] W. Schotte, Ind. Eng. Chem. Res., 26 (1987) 300.
[7] J.H. Seinfeld, Atmospheric Chemistry and Physics of Air Pollution, Wiley, New York, 1986.
[8] F. Ricou and D.R. Spalding, J. Fluid Mech., 11 (1961) 21.
[9] G. Ooms, Atm. Environ., 6 (1972) 899.
[10] G.A. Briggs, Plume Rise, AEC Critical Review Series TID-25075, National Information Service, U.S. Department of Commerce, 1969
[11] J.C. Kaimal, J.C. Wungaard, D.A. Haugen, O.R. Cote and Y. Izumi, J. Atmos. Sci., 33 (1976).
[12] K.W. Schatz, G.R. Jersey, M.K. Chalam and D.W. Johnson, Presented at the A.I.Ch.E. Summer National Meeting, Seattle, 1993.
[13] G.R. Jersey, K.W. Schatz, M.K. Chalam and R. Muralidhar, Presented at the A.I.Ch.E. Summer National Meeting, Seattle, 1993.
[14] R. Muralidhar, G.R. Jersey, J.E. Child and S. Sundaresan, manuscript in preparation, 1994.
[15] D.J. Holve, T.L. Harvill, K.W. Schatz and R.P. Koopman, J. Loss Prev. Process Ind., 3 (1990) 234.
[16] R.C. Reid, J.M. Prausnitz and B.E. Polling, The Properties of Gases and Liquids, McGraw-Hill, New York, 4th edn., 1987.
[17] T.E. Daubert and R.P. Danner, Physical and Thermodynamic Properties of Pure Chemicals – Data Compilation, NSRDS/AIChE, Hemisphere, 1989.